Faculty of Electrical Engineering
Department of Control Engineering

Bachelor's thesis

Emergency Landing Guidance for an Aerial Vehicle with a Motor Malfunction

Jakub Sláma

May 2018
Supervisor: doc. Ing. Jan Faigl, Ph.D.
Supervisor specialist: Ing. Petr Váňa

"A mile of road will take you a mile,
but a mile of runway can take you anywhere."

ANONYMOUS AVIATION WISDOM

BACHELOR'S THESIS ASSIGNMENT

I. Personal and study details

Student's name: **Sláma Jakub**   Personal ID number: **457224**

Faculty / Institute: **Faculty of Electrical Engineering**

Department / Institute: **Department of Control Engineering**

Study program: **Cybernetics and Robotics**

Branch of study: **Systems and Control**

II. Bachelor's thesis details

Bachelor's thesis title in English:

Emergency landing guidance for an aerial vehicle with a motor malfunction

Bachelor's thesis title in Czech:

Navádění letadla s poruchou motoru na nouzové přístání

Guidelines:

1. Familiarize yourself with existing planning approaches for emergency landing [1, 2, 3].
2. Propose a simplification of flights dynamics [4] of airplanes to estimate energy consumption during an emergency landing with a malfunctioned motor.
3. Extend the existing Dubins Airplane model [5] for emergency landing of fixed-wing aerial vehicles and calculation of a height loss during the landing.
4. Propose and develop trajectory planning algorithm for emergency landing of small aircraft which calculates airplanes minimal safety height over terrain for its emergency landing.
5. Evaluate performance of the proposed solution and discuss the results regarding realistic scenarios.

Bibliography / sources:

[1] Pillar Eng. Path planning, guidance and control for a UAV forced landing. Ph.D. dissertation Queensland University of Technology, 2011.
[2] Choudhury, Sanjiban, Sebastian Scherer, and Sanjiv Singh. RRT*-AR: Sampling-based alternate routes planning with applications to autonomous emergency landing of a helicopter, ICRA, 2013, pp. 3947-3952.
[3] Desaraju, Vishnu R., et al. "Vision-based landing site evaluation and informed optimal trajectory generation toward autonomous rooftop landing." Autonomous Robots, 39(3):445-463, 2015.
[4] Durham, Wayne. Aircraft flight dynamics and control. John Wiley & Sons, 2013.
[5] Hamidreza Chitsaz and Steven M. LaValle, "Time-optimal paths for a dubins airplane", in 46th IEEE Conference on Decision and Control. IEEE, 2007, pp. 2379 - 2384.

Name and workplace of bachelor's thesis supervisor:

doc. Ing. Jan Faigl, Ph.D.,   Artificial Intelligence Center,   FEE

Name and workplace of second bachelor's thesis supervisor or consultant:

Ing. Petr Váňa,   Dept. of Computer Science and Eng.,   FEE

Date of bachelor's thesis assignment: **31.01.2018**   Deadline for bachelor thesis submission: **25.05.2018**

Assignment valid until: **30.09.2019**

_____
doc. Ing. Jan Faigl, Ph.D.
Supervisor's signature

_____
prof. Ing. Michael Šebek, DrSc.
Head of department's signature

_____
prof. Ing. Pavel Ripka, CSc.
Dean's signature

III. Assignment receipt

The student acknowledges that the bachelor's thesis is an individual work. The student must produce his thesis without the assistance of others, with the exception of provided consultations. Within the bachelor's thesis, the author must state the names of consultants and include a list of references.

.

Date of assignment receipt   Student's signature

Declaration

I hearby declare that the presented work was developed independently ant that I have listed all sources of the information used within it in accordance with the methodical instructions for observing the ethiclal principles in the preparation of university theses.

Prague, May 25, 2018

....
Jakub Sláma

Acknowledgement

Abstract

The total loss of thrust on a fixed-wing aircraft is very dangerous situation for the pilots. It forces them to choose a suitable landing site which is reachable and to perform emergency landing. The time for selecting the landing site is limited by the aircraft actual altitude and if an incorrect decision is made or if the correct decision is not made fast enough, it may have fatal consequences. Therefore, we propose a novel algorithm to select the best landing site and the corresponding most suitable gliding trajectory. The proposed algorithm is based on asymptotically optimal variant of the Rapidly-exploring Random Tree (RRT*) approach that is modified such that all the reachable landing sites are evaluated simultaneously during the whole flight, even before any loss of thrust is detected. If the total loss of thrust occurs, the best landing site and a feasible gliding trajectory towards it is proposed to the pilots almost instantly. The feasibility of the found solution is ensured by the use of the deduced model of a gliding aircraft based on Cessna 172.

Keywords: emergency landing; trajectory planning; loss of thrust; gliding aircraft

Abstrakt

Celková ztráta tahu u letadel je velmi nebezpečná situace, která vyžaduje zvolit vhodnou dosažitelnou přistávací plochu a provést nouzové přistání bez motoru. Čas na zvolení místa přistání je omezený aktuální výškou letadla, a pokud je zvolena nevhodná plocha pro přistání a nebo pokud není zvolena včas, může to vést k fatálním následkům. V práci proto navrhujeme novou metodu průběžného plánování bezpečných přistávacích trajektorií, která je schopná zvolit nejvhodnější místo pro přistání spolu s příslušnou trajektorií samotného přistání. Všechna dosažitelná místa přistání se průběžně vyhodnocují po celou dobu letu, a tedy i před tím, než dojde ke ztrátě tahu. V takovém případě je nejvhodnější místo přistání a příslušná trajektorie pro klouzavé nouzové přistání pilotovi nabídnuta téměř okamžitě. Proveditelnost nalezeného nouzového přistání je zaručena použitím odvozeného modelu plachtícího letounu založeného na letadle Cessna 172.

Klíčová slova: nouzové přistání; plánování trajektorií; ztráta tahu; plachtící letadlo

Used Abbreviations

CTU	Czech Technical University in Prague
EST	Eastern Standard Time
RRT	Rapidly-exploring Random Tree
UAV	Unmanned Aerial Vehicle

Used Symbols

Γ	Emergency landing trajectory
Δ_{max}	Steer constant
ϵ	Span efficiency factor
θ	Pitch angle
θ^g	Pitch angle during an optimal glide
κ	Trajectory curvature
Ξ	Set of landing sites
ξ	Landing site
ξ_*	Selected landing site
$\widehat{\xi_*}$	Set of all configurations above selected landing site ξ_*
ρ	Air density
φ	Roll angle
ψ	Heading angle
$\mathcal{A}$	Aircraft minimum altitude for a safe landing
b	Wingspan
$\mathcal{C}$	Configuration space of aircraft configurations q
C_{D}	Drag coefficient
C_{D0}	Coefficient of geometric drag
C_{L}	Lift coefficient
$\mathbf{D}$	Drag
$\mathcal{E}$	Euclidean distance function
$\boldsymbol{E}$	List of edges within a graph
G	Graph
g	Gravitational acceleration
$\mathcal{H}$	Altitude loss function
h	Height above terrain

k	Lift-induced drag coefficient
k_{nn}	Number of nearest chosen samples in proposed algorithm
$\mathcal{L}$	2D length of a trajectory segment
$\mathbf{L}$	Lift
m	Aircraft mass
p	Point
Q_{near}	Set of k_{nn} nearest neighbors
q	Aircraft configuration
$\widehat{q}$	All configurations identical to q except the altitude
$\tilde{q}$	Simplified aircraft configuration
R	Turning radius
S	Wing area
$\mathcal{T}_{\mathrm{alt}}$	Aircraft minimum non-colliding altitude
$\mathbf{T}$	Thrust
u	Control input
v	Forward speed of the aircraft
V	List of vertices in a graph
$\mathbf{W}$	Weight

Contents

List of Figures

List of Tables

List of Algorithms

A Tale of Modern Aviation

Flying has been one of the biggest desire of the mankind. People have always admired birds and their ability to fly. Therefore, the history is full of myths and legends about flying. The most known one is probably *The Myth of Icarus* which is dated back to Ancient Greece. Except for the myths and legends, there has been an enormous number of flying attempts which often ended up by failure, injury or even by a death of a "pilot". Those experiments included kite flying, tower jumping, flying with bird-like wings, etc. It took almost two thousand years to the first successful flight of a heavier-than-air aircraft.

Figure 1.1: The first successful manned engine-powered flight performed by the Wright brothers on December 17, 1903. The flight lasted 12 seconds and covered 36.6 meters. Credits: Wikipedia[1]

The kite may be the oldest man-made aircraft which was invented in China around 5th century BC. As Ancient and Medieval Chinese sources suggest, those kites were used for measuring distances, testing the wind, signalling, sending messages and even for men lifting. But still, it was just an uncontrollable device. Another very popular flying attempts included tower jumping with bird-like wings attached to a body. In those days, the theory of lift, stability, and control was unknown, so those attempts very often ended up in a serious injury or even death. Later on, in the Renaissance, some ideas based on bird flights' observation

---

[1]`https://upload.wikimedia.org/wikipedia/commons/0/09/Wrightflyer_highres.jpg`

began to appear. The most notable of these was Leonardo da Vinci whose ideas remained unknown for another three centuries. More the mankind understood the nature and its laws, the more realistic experiments took place.

A milestone was reached in 1783 with first successful balloon flights. On June 4, the Montgolfier brothers demonstrated their first hot air balloon flight at Annonay, France. There were not any passengers nor pilots onboard for safety reasons. On August 27, Jacques Charles and the Robert brothers launched the world's first hydrogen-filled balloon from Paris, France. Later on, on October 19, the Montgolfier brothers demonstrated the first manned flight, and on October 21, they launched the first flight with passengers. The first manned flight of the hydrogen-filled balloon was launched on December 1. This year adumbrated a development of balloons and airships.

Another huge milestone was reached on December 17, 1903, when the Wright brothers successfully flew the manned engine-powered fixed-wing aircraft for the first time. Even though the first flight lasted only 12 seconds and covered only 36.6 meters, it started the era of modern aviation as we know it today. Their first flight is depicted in Fig. 1.1.

1.1 Rocket Evolution of Aircraft

Although the first successful manned powered flight took place only a century ago, the aviation has undergone tremendous development. During the last century, aircraft changed from small simple wooden constructions covered with fabrics into huge carbon-fabrics and highly sophisticated machines capable of transporting hundreds of people at once. Due to that, modern aircraft are requested to be highly reliable and safe. Extensive tests are held during a development of a new aircraft to guarantee its capabilities. An example of Airbus A350 XWB, Airbus first mainly-composite-aircraft, undergoing one of the tests during its development can be seen in Fig. 1.2.

Figure 1.2: Airbus A350 XWB during a water ignition test. This test is held to confirm the aircraft ability to operate safely in wet conditions, i.e., engines will not go off in a heavy rain. Credits: Airbus[2]

In the beginning, aircraft were not capable of long flights. In 1914, the first fixed-wind aircraft air service started in the USA only few years after the successful flight of the Wright brothers. The flight was 34 km long and it was scheduled between St. Petersburg, Florida and Tampa, Florida. In 1919, the first nonstop transatlantic flight became a reality. Only

---

[2]`https://youtu.be/eQgdOAC2aNM?t=3m10s`

20 years later, the first jet-engine fixed-wing aircraft Heinkel He 178 took-off, and the first commercial jetliner de Havilland Comet took-off in 1949. The very first transatlantic jet service started only nine years later, in 1958. We have also witnessed a race for breaking the sound barrier. The first aircraft that successfully broke the sound barrier is Bell X-1 piloted by Charles "Chuck" Yeager on October 17, 1947. The first commercial supersonic aircraft, nothing else than the world-famous Concorde, took-off for the first time in 1969 and it got in a regular service seven years later, in 1976.

This rocket development of aviation make the world much smaller; today, we can get anywhere in the world within a single day. It is an enormous business as well. According to [IATA, 2017a, IATA, 2017b], there were approximately 101 thousand daily flights and 62.7 million work positions supported by the air transport industry including 9.9 million directly created jobs worldwide, in 2017. Moreover, 11.2 million of passengers as well as 171.2 tons of cargo with a value of $17.5 billion travelled via air every day. Modern aviation is a true marvel.

1.1.1   General Aviation

General aviation is a term used for all civil other-than-scheduled air services. This type of transportation is quite frequent nowadays. For example, it is very popular in North America, where people often need to travel long distances. It is very similar to driving; a person who can successfully finish flying lessons and receive a flying license is allowed to fly a certain category of aircraft. An example of general aviation aircraft is depicted in Fig. 1.3. In contrast to airliners, which are piloted by professional pilots who are extensively and periodically trained, general

Figure 1.3: General aviation flights, i.e., non-scheduled civil air flights, are very common, mainly in North America, where people often travel very long distances. Among the popular aircraft is Cessna Skyhawk, produced by Textron Aviation. Credits: Textron Aviation[3]

aviation is not under such a control. That means general aviation pilots are more likely to make a mistake, to not handle correctly dangerous situations such as bad weather, etc., which results in a higher risk of an accident. On top of that, most of the general aviation flights are flown under *visual flight rules* meaning that the pilot orients visually by surrounding terrain,

---

[3]http://cessna.txtav.com/-/media/cessna/images/aircraft/piston/skyhawk/exterior-gallery/dbsg_0418.ashx

and so it is not vectored by an air traffic controller. Thus, in a case of an emergency, general aviation does not receive as high amount of support as airliners do.

1.2 Dawn of UAVs

Although modern aircraft are true marvels of technology, their operations have drawbacks as well. First of all, modern aircraft are very reliable, safe, and effective but also very expensive. Moreover, they are piloted by humans so they must be big enough to seat at least one person which increases their size and thus operational costs. Another drawback of aircraft are pilots themselves. Paying a pilot is not cheap. They also constitute a danger to an aircraft as a human pilot can misunderstand receiving data or commands, for example. Last but not least, people tend to lose attention when doing monotone repetitive activities. These drawbacks are among the reasons why unmanned aerial vehicles (UAVs) have been invented. Examples of UAVs used at Czech Technical University in Prague (CTU) are shown in Fig. 1.4.

(a) Fixed-wing

(b) Rotary-wing Credits: CTU

Figure 1.4: Examples of UAVs used at CTU. They serve as a platform for various experiments, such as path planning, autonomous navigation, and object tracking.

There are many versions of UAVs, from remotely controlled ones up to high-end fully autonomous vehicles which are fully capable of their missions. All of them bring cheaper, safer, and easier operations than classic aircraft. They are literally getting into the every aspect of our lives and they have an enormous potential for a future use. Thanks to their abilities and the effort invested into their development, we can expect we will meet them during our everyday lives much more often.

1.3 Dark Side of Flying

Although modern aircraft are technological miracles and they are very safe and reliable as well, malfunctions and accidents happen. Any problem in an aircraft is much more dangerous than for example in a car; if any problem arises in a car, the driver can simply pull over and solve it, however, in an aircraft, the pilot simply cannot do that. Any problem must be solved in flight, or at least the pilot has to land safely. In the opposite case, the flight can end up in an accident. Apparently, pilots are trained to manage a lot of emergency situations, but every emergency situation is specific. Hence, it is up to the pilot's knowledge, skills and

even a bit of luck. Professional pilots are trained more extensively and much more often than hobby pilots, and therefore, the general aviation is more likely to end up in an accident than airliners, according to [Kenny, 2017]. These drawbacks and the need for addressing an emergency landing path planning can be demonstrated on several accidents from the past.

1.3.1 UA1549: Miracle on the Hudson

On January 15, 2009, New York was experiencing nice, chilly, and busy afternoon; it was -6 °C with broken clouds and a gentle breeze. LaGuardia Airport was hectic as usual and US Airways flight 1549 was already boarded. This flight was scheduled from New York's LaGuardia Airport to Charlotte Douglas, North Carolina. It was a busy flight as the Airbus A320 was almost full with 150 passengers, three cabin crew members and two experienced pilots on board [Hersman et al., 2010]. The pilot-in-command was 57-year-old Chesley B. "Sully" Sullenberger, a former fighter pilot who has logged 19,663 total flight hours, including 4,765 hours in an A320; he was also a glider pilot and an expert on aviation safety. The first officer was Jeffrey B. Skiles, 49 years, who had flown 15,643 flight hours during his career but it was his first flight in A320 since receiving a qualification for it.

The aircraft was cleared for take-off at 15:24:54 EST, and it was airborne one minute later. The weather was nice with visibility of 10 miles, as the crew noticed as well and the pilot-in-command Sullenberger remarked: *"What a view of the Hudson today."* Less than three minutes from take-off, things went seriously wrong. The aircraft struck a flock of Canada geese at the altitude of only 2,818 ft (859 m) which resulted in the almost total loss of thrust. Realizing both engines shut down, Sullenberger took control of the aircraft and Skiles went through the checklist for an engine restart. The aircraft continued to climb for another 19 seconds after the collision reaching the altitude of 3,060 feet (930 m) and then it started a glide descent. At 15:27:33 EST, only 22 seconds after the collision, Sullenberger transmitted a mayday call: *"Mayday mayday mayday. Uh this is uh Cactus[4] fifteen thirty nine, hit birds. We've lost thrust (in/on) both engines. We're turning back towards LaGuardia."* Notice the experienced captain wrongly identified their flight as UA1539 instead of UA1549 during the mayday call. An air traffic controller gave them a path towards LaGuardia airport, but Sullenberger responded *"Unable."* A few moments later, he asked for a clearance to land at nearby Teterboro Airport, New Jersey. While the air traffic controller was arranging the landing clearance, captain Sullenberger prepared passengers for the worst by words any passenger would not like to hear: *"This is the Captain, brace for impact."* Seconds later, they received the clearance to land at Teterboro's runway 1, however, realizing the vastness of the problem, captain Sullenberger refused it. The air traffic controller asked which runway he would like to land. Sullenberger, fully employed by flying a gliding aircraft over Manhattan, simply answered: *"We're gonna be in the Hudson."* The aircraft flew over George Washington Bridge lower than 270 m. A few moments later, 213 seconds after the collision with a flock of Canada geese, the aircraft ditched into the Hudson River.

Emergency landings on water are the most dangerous ones because even a small deviation from the optimal path can cause a disaster. Luckily, this was not the case, and the aircraft successfully landed on the river. As the evacuation started, people were facing another huge danger – hypothermia. Water had only 5 °C but thanks to nearby ships and ferries, all passenger were out of water by 15:55, only 25 minutes after the ditching. All 155 people on board survived; only five passengers suffered serious injuries, 95 of them sufferer minor

---

[4]Cactus is the callsign of US Airways used for communication between pilots and air traffic controllers.

injuries, and 55 of them got out not injured at all. Therefore, this flight was nicknamed Miracle on the Hudson. The ditched aircraft on the Hudson River is depicted in Fig. 1.5.

Figure 1.5: US Airways flight 1549 after an emergency landing on the Hudson River. This Airbus A320 had to land on a river in the middle of New York after a collision with a flock of Canada geese causing almost the total loss of thrust. Credits: Wikipedia[5]

Later on, during the investigation, it was shown pilots had very little time for analyzing the situation and choosing the most suitable landing site. According to simulations [Paul et al., 2017], it was possible to avoid water ditching and land safely at nearby airports up to 30 seconds after the unexpected bird strike. However, such a decision is extremely difficult for human pilots under such stressful conditions when the technical problem itself has to be identified. Unfortunately, in the time when pilots realized they lost thrust in both engines without a chance to restart them and an emergency landing would be necessary, they did not have enough height to land at any nearby airport safely and, obviously, their decision to land on the Hudson River was the best possibility.

This accident is an example how important it might be to make the right decision and start the emergency landing to the most suitable landing site as soon as possible. Otherwise pilots may get into a situation when they would be unable to land at any landing site. In such a situation, pilots could definitely land safely on any different place, but such an emergency landing is much more dangerous posing a high risk of an accident.

1.3.2 AC143: Gimli Glider

Air Canada Boeing 767 departed from Montreal on July 23, 1983, heading to Edmonton with a stopover in Ottawa as Air Canada flight 143 [Lockwood, 1985]. The pilot-in-command was Robert Pearson, 48, and the first officer was Maurice Quintal, 36. Pearson was a highly experienced pilot with more than 15,000 flight hours in his log. Quintal was also experienced, he has accumulated about 7,000 flight hours.

On that day, everything went perfectly, except few details. For example, gauges indicating fuel levels were inoperative due to an electrical fault indicated on the instrument panel and in a log in the aircraft logbook. The amount of fuel in tanks was loaded into the flight computer at the airport so it should not be a problem. The aircraft was flying at the altitude of 41,000

---

[5]`https://upload.wikimedia.org/wikipedia/commons/0/0f/Plane_crash_into_Hudson_River_%28crop%29.jpg`

feet (12.5 km) over Red Lake, Ontario when a warning system indicating fuel pressure problem on the aircraft left side sounded. Assuming a fuel pump stopped working, pilots turned it off because gravity should still feed the engine with fuel. A few moments later, the second alarm indicating fuel pressure problems on the right side sounded. Within few seconds, the left engine failed. The flight had to divert to Winnipeg and while pilots were preparing for a single-engine emergency landing, the cockpit alarm sounded once more with a specific sound indicating *all engines out.* However, flying with all engines out was not expected to ever occur, and so this was not covered in pilots' training. Therefore, no one in the cockpit recognized this specific alarm. Seconds later with the right engine failed as well, the aircraft lost all power and almost all instruments in the cockpit went black. Only few basic flight instruments stayed alive but unfortunately vertical speed indicator, which indicates the aircraft rate of descent, allowing pilots to estimate how far they can glide, was not among them. To make it worse, engines powered the hydraulic system needed for controlling the flight, too. Luckily, aircraft such as this Boeing 767 are required to sustain such a loss of power, and so they have a small ram air turbine which keeps the hydraulic system alive. However, this turbine relies on the forward motion of the aircraft. As the aircraft was slowing down before landing, the generated power available for controlling the aircraft decreased, and thus made it harder to control the aircraft.

The aircraft was at 35,000 feet (11 km) at the time the second engine failure. They immediately started to search in the emergency checklists for a section on flying the aircraft without engines, but such a section did not exist as no one ever expected the occurrence of such a failure. Captain Pearson was an experienced glider pilot familiar with gliding techniques never used in commercial aviation. He had estimated the optimal glide speed allowing them to fly the furthest distance and with the help of an air traffic controller, pilots estimated their glide ratio as 12:1, meaning that for every descended meter, they flew 12 meters in the distance. Having this information, pilots decided to land at a former RCAF Station Gimli. However, no one of them knew that the part of the former airbase was transformed into a racing track complex.

Figure 1.6: Air Canada Boeing 767 after an emergency landing at the former RCAF Station Gimli. The aircraft was forced to land there after it ran out of fuel. Credits: Wikipedia[6]

Not having the power, pilots had to use gravity for lowering the gear. Moreover, pilots were not able to use flaps nor the air brake due to the lack of power, and as they were getting

---

[6]`https://upload.wikimedia.org/wikipedia/en/2/24/Gimli_glider.JPG`

closer to the runway, it was getting clear their altitude is too high and they are too fast posing the risk of running off the runway before stopping. They briefly considered making a 360-degrees turn helping them to lose height and slow down, but they did not have enough height for a safe landing after such a turn. Captain Pearson decided to make a forward slip; a maneuver used by glider pilots to lose the height faster without increasing the speed. Nose gear did not lock up, so it collapsed during breaking that resulted in the aircraft skid on its nose increasing the drag and slowing faster. Thanks to all of that, the aircraft landed safely, and everyone on board and the ground survived, even though there were races on the closed airport which was full of campers. There were only ten minor injuries caused during the evacuation. The aircraft after the emergency landing is captured in Fig. 1.6.

It showed up during the investigation that a human error was to blame for this accident. The pilots calculated the amount of needed fuel in kilograms, but ground staffs were using the imperial unit system and fueled the aircraft with the same amount of fuel, but in pounds. No one had noticed, and so the aircraft had less than a half of the required fuel. Gauges indicating fuel levels were not working and pilots relied on the prediction made by the flight computers. Since data loaded into them did not correspond with the real amount of fuel in the tanks, the pilots had not a chance to notice they are running low fuel when airborne.

This accident is a textbook example of a human mistake which happened due to a lack of attention during a routine process. Moreover, this accident showed there are more ways how to treat an excess altitude or speed during a gliding landing.

1.3.3 Small Aircraft Making Big Crashes

General aviation is more vulnerable to accidents than commercial aviation because much more people can obtain a license to fly a small aircraft, its regulation is not so strict, and pilots are not as experienced as commercial ones [Kenny, 2017]. General aviation flights are not as long

Figure 1.7: Crashed Cessna 172 near Nome, Alaska. Credits: KNOM radio mission[7]

as airliner flights. Thus, the general aviation has higher numbers of landings and take-offs. Take-offs and landings are the most dangerous parts of a flight which increases the overall dangerousness of general aviation. Last, but not least, general aviation aircraft are not as safe as airliners, for example concerning withstanding weather due to their smaller sizes and limited equipment. One of the general aviation aircraft crashes can be seen in Fig. 1.7.

---

[7]`http://www.knom.org/wp/wp-content/uploads/2017/03/Plane-Crash_Hastings-Creek-1216x912.jpg`

A powerplant failure was the most common mechanical cause of fixed-wing non-commercial general aviation aircraft accidents in 2014 with 63 of them, from which 12 of them were fatal. In the same year, about 80% of all fatal accidents caused by mechanical problems involved the in-flight loss of thrust [Kenny, 2017]. Those were caused by various problems, such as bird strikes, mechanical problems, fuel exhaustions, etc.

1.4 Guidance System

Time-critical decisions under stressful circumstances can be very hard for humans posing a risk of a wrong decision and inability to decide in time. An example of such a situation is US Airways flight 1549, see Sec. 1.3.1, in which pilots missed the time for a diversion to LaGuardia Airport after a collision with a flock of birds and were forced to ditch into the Hudson River. However, such a decision is easy for computers.

Developing a guidance system capable of supporting pilots' decision based on the all currently available computational machinery in cases similar to US Airways flight 1549 and other accidents is our motivation to study the herein presented trajectory planning problem for an emergency landing of a fixed-wing aircraft with an engine malfunction. Our goal is to provide fast and reliable information about all possible nearby landing sites to pilots in the total loss of thrust scenarios. In these scenarios, pilots are forced to choose the most suitable landing site as the aircraft is gliding due to the loss of thrust. Airports with longer runways and emergency resources are preferred. However, the most important question is whether the aircraft has a sufficient altitude for gliding safely to the chosen landing site.

Thus, we propose a novel method for an emergency trajectory planning which is based on the RRT* algorithm. This algorithm is capable of finding a feasible trajectory, if such a trajectory exists. We deduce a mathematical model of the gliding aircraft to appropriately describe its descent. Moreover, we devise modifications of the RRT* algorithm so it can determine the landing site together with the gliding trajectory towards it.

Related Work

If an aircraft is affected by the total loss of thrust, it needs to glide to a suitable landing site. Such a glide is quite risky because any wrong decision can cause the aircraft gets in a situation that it cannot reach any landing site. Developing a system helping pilots with such a decision calls for the capability of planning an emergency landing trajectory towards the most suitable landing site with regards to aircraft motion constraints. This capability can be divided into several categories: landing sites detection and determination, a capability of finding a feasible trajectory between two configurations of the aircraft, and state-space search techniques for obstacle avoidance.

2.1   Landing Sites Detection and Determination

A landing site determination is probably the most crucial part of an emergency landing because if unsuitable landing site is chosen, the aircraft can crash. Moreover, some landing sites pose more risk to the landing than others, and so the most suitable one has to be chosen. A method of visual detection of landing sites is proposed in [Mejias and Fitzgerald, 2013]. The method relies on the edge detection in an RGB image. Then, the edges are growth and spare areas are found in the arose image. These areas are tested in the original RGB image to throw away areas which probably correspond to areas unsuitable for landings. Found areas are considered to be a possible landing site.

[Desaraju et al., 2015] propose a method for visual detection of possible landing sites on rooftops for micro-aerial vehicles. They propose to use a 3D site reconstruction and find all enough flat sites providing sufficient space for an emergency landing.

[Humbard and Putman, 2007] propose a method of a visual aid for pilot's decision about the most suitable landing site. The principle is that a reachability cone is calculated for each known possible landing site near the aircraft and results are shown to the pilot; so, she/he can clearly see which landing sites are reachable. A reachability cone is simply a cone from which the plane can glide to the desired point, in this case to the landing site. The reachability cone is determined by the glide ratio of the aircraft. Any obstacles nor terrain are not taken into account.

The authors of [Meuleau et al., 2009] propose a method of the landing site determination for airliners based on the probability of failed landing and its consequences regarding possible

damage and loss of lives. Their method has been implemented and tested on the NASA simulator for Boeing 757/767 aircraft category [Meuleau et al., 2011].

[Atkins, 2010] states that today airliners systems know all key factors for emergency landing site determination: airports and their runways, nearby obstacles and traffic, wind speed and direction, etc. They develop a method for determination of the best landing sites, show them to pilots and help them with a decision where to land. They evaluate their proposed method on data from the US Airways Flight 1549, which was forced to land on the Hudson River in the middle of New York after the total loss of thrust.

2.2   2D Path Planning

In total loss of thrust scenarios, the task is to optimize the altitude loss. Hence, the trajectory is given by its 2D projection and its vertical profile is determined by the aircraft gliding capabilities.

2.2.1   Trajectory Generation

The problem of finding the shortest curvature-constrained path in a plane was firstly studied in [Dubins, 1957]. The considered curvature-constrained vehicle with a constant forward speed can be described by

$$\begin{bmatrix} \dot{x} \\ \dot{y} \\ \dot{\psi} \end{bmatrix} = v \begin{bmatrix} \cos\psi \\ \sin\psi \\ \frac{u_\psi}{R_{\min}} \end{bmatrix} , \tag{2.1}$$

where v is the vehicle constant forward velocity, ψ is its heading angle, $u_\psi = [-1, 1]$ is the control input, and $R_{\min}$ is the minimum turning radius. Such a model is called **Dubins vehicle**. In [Dubins, 1957], it is proved that a shortest trajectory for such a vehicle in a plane between two points with prescribed heading angles is either

- CCC maneuver,

- CSC maneuver,

where C stands for a circular segment using $R_{\min}$ and S stands for a straight line segment. Moreover, Dubins showed that CCC maneuvers can exist only if the maneuver end points are closer than four times the minimum turning radius $R_{\min}$. An example of these maneuvers can be found in Fig. 2.1. The closed-form solution exists, and so finding a shortest curvature-constrained trajectory in 2D is fairly simple.

[Chaudhari et al., 2014] extended Dubins maneuver by allowing different turning radii for each circular segment. They also showed its closed-form solution. Besides, any parametric curves can be used for path planning. [Choi et al., 2008] study the use of quadratic Bézier curves for a trajectory generation. A Bézier curve is a parametric curve defined by at least start and end points and two other points. Together, they define heading angles at start and end points and the curve shape itself. However, we are not able to directly construct the Bézier curve with the minimum turning radius; we can only check if the final trajectory satisfies curvature constraints.

[Connors and Elkaim, 2007a] study splines for path planning for mobile robots and report the evaluation results in [Connors and Elkaim, 2007b]. Splines are another parametric curves

(a) CSC maneuver   **(b)** CCC maneuver
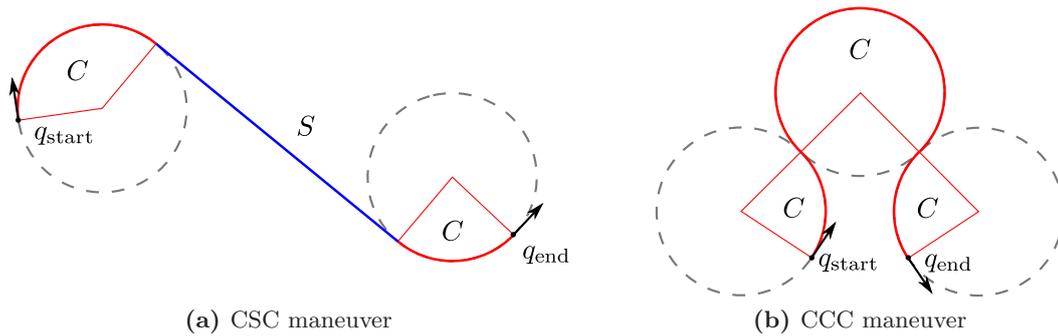
Figure 2.1: An example of Dubins maneuvers in a plane.

defined by the start and end positions and an arbitrary number of supporting points, giving together start and end heading angles and the shape of the curve. The curve is based on polynomial methods on each segment defined by two points. Examples of a Bézier and spline curves are depicted in Fig. 2.2.

(a) Bézier curve   **(b)** Spline curve
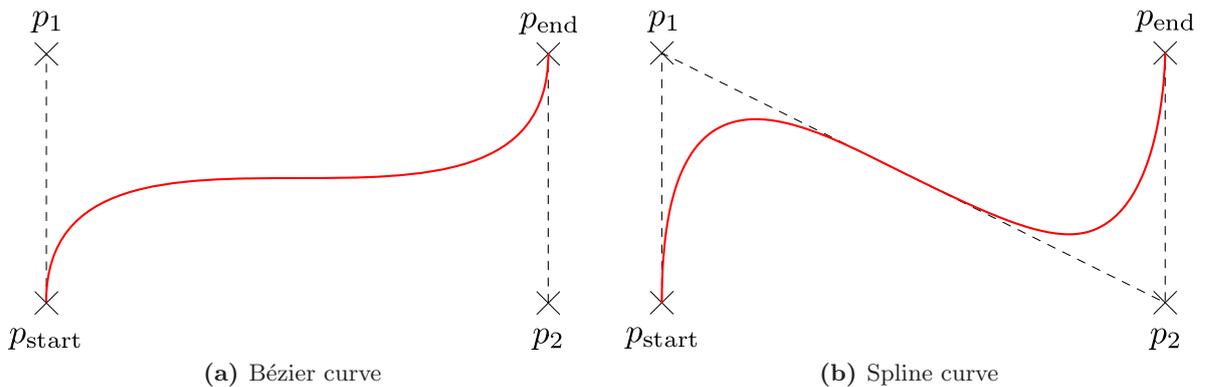
Figure 2.2: An example of smooth trajectories based on parametric curves. Such a trajectory allows smooth changes in acceleration of a vehicle unlike the Dubins maneuver. However, such a trajectory is more difficult to compute and usually we cannot set the minimum turning radius in advance.

2.2.2 Energy Models Used for Trajectory Vertical Profiles

Models describing aircraft dynamics are used for the determination of the vertical profile along a 2D trajectory. One of the most sophisticated energy-based model is called Base of Aircraft Data (BADA) model and it is developed by Eurocontrol. BADA model version 3.13 specifies operation performance parameters, airline procedure parameters, and performance summary tables for 519 aircraft and it was developed for a use in trajectory simulation and prediction algorithms within the domain of Air Traffic Management [Nuic, 2015]. This model is based on the total energy model, counting with altitude and airspeed changes. Moreover, the model takes changes in atmosphere attributes into account, due to its primary aim on airliners. It also counts with changes in aircraft configurations. Nevertheless, it does not take changes caused by turning into account. These changes are quite small, and airliners fly most of the flight straight. Therefore, they are neglected in this model.

[Paul et al., 2017] deduce an energy model for Airbus A320 involved in the US Airways flight 1549 accident. They also show similar model for Cessna 172 for a comparison. Another energy model for Airbus A320 is desbrided in [Atkins, 2010].

2.3 Path Planning Algorithms

Finding a suitable landing path means that we need to find such a path for any start configuration. Thus, we need to assign a solution to any configuration in a continuous space. In general, we do not have such a possibility as we work with discrete objects and that is why methods for state-space searching have been developed.

2.3.1 RRT-based Algorithms

[LaValle, 1998] came with a Rapidly-exploring Random Tree (RRT) algorithm which can search the state-space and take motion constraints into account. The main idea of the algorithm is to randomly sample the space, test samples if they are feasible and if so, connected them into a tree structure that incrementally (but randomly) grows towards the goal location. A pseudo-code of this algorithm can be found in Algorithm 1.

The initial configuration is inserted into the tree as the first node assuming it is a valid state. Then in the first step of each iteration, a non-colliding random configuration is chosen from the configuration space $\mathcal{C}$ such that $x_{\text{rand}} \in \mathcal{C}_{\text{free}}$ and its closest node from the tree is found by the `NearestNeighbor()` procedure. After that, the needed input u moving the object from the configuration q_{rand} to q_{near} is determined and a new configuration is created in the procedure `NewConfiguration()`. The new configuration is added into the tree, and the whole cycle is repeated until the desired number of nodes in the tree is reached.

Algorithm 1: RRT as Proposed by [LaValle, 1998]

> **Input:** q_{init} – initial configuration
> **Input:** K – number of desired vertices
> **Input:** Δt – time step
> **Output:** G – tree

1 `Init`(G, q_{init})
2 for $k = 1$ **to** K **do**
3 $\quad$ $q_{\text{rand}} \leftarrow$ `RandomConfiguration()`
4 $\quad$ $q_{\text{near}} \leftarrow$ `NearestNeighbor`(q_{rand}, G)
5 $\quad$ $u \leftarrow$ `SelectInput`$(q_{\text{rand}}, q_{\text{near}})$
6 $\quad$ $q_{\text{new}} \leftarrow$ `NewConfiguration`$(q_{\text{near}}, u, \Delta t)$
7 $\quad$ `AddVertex`(q_{new}, G)
8 $\quad$ `AddEdge`$(q_{\text{new}}, q_{\text{near}}, u, G)$

Unfortunately, it was shown that the RRT algorithm converges to non-optimal solution with probability one under certain conditions [Karaman and Frazzoli, 2010]. The new configuration is connected to the closest configuration in the tree. However, the overall cost might not be the lowest possible. Nevertheless, it finds the first feasible solution. Thus, [Karaman and Frazzoli, 2010] proposed a modification called RRT* and proved its asymptotic optimality under specific conditions. In general, we can say the solution improves with

time. The algorithm follows the same randomized growing of the tree, but it enables to improve the solution by connecting nodes in the tree for better trajectory. Besides, the algorithm consider results on the Random Geometric Graph (RGG) proposed by [Penrose, 2003] to show asymptotic optimality with increasing number of samples, which is basically related to the updating the neighboring function (utilized in the reconnecting). The RRT* algorithm is summarized in Algorithm 2.

First, the nearest neighbor is extended towards the random sample. If the extension is longer than the maximum allowed step $\Delta_{\max}$, the maneuver is shortened and a new sample is made at its end, which is made in the $\mathtt{Steer}()$ procedure. Then, the new vertex q_{new} is connected to the vertex that incurs the minimum accumulated cost up to the new vertex q_{new} and which lies within the set Q_{near} of the k_{nn} closest vertices returned by the procedure $\mathtt{Near}()$ instead of connecting it to the closest vertex. Finally, the vertices in Q_{near} are tested in the $\mathtt{Rewire}()$ procedure if they can be accessed through the newly inserted vertex with a smaller cost.

Algorithm 2: RRT* as Proposed by [Karaman and Frazzoli, 2010]

Input: q_{init} – initial configuration
Input: Δt – time step
Output: G – tree

1   $\mathtt{Init}(G, q_{\text{init}})$
2   **while** terminal condition is not met **do**
3     $q_{\text{rand}} \leftarrow \mathtt{RandomConfiguration}()$
4     $q_{\text{nearest}} \leftarrow \mathtt{Nearest}(q_{\text{rand}}, G)$
5     $q_{\text{new}} \leftarrow \mathtt{Steer}(q_{\text{nearest}}, q_{\text{rand}})$
6   **if** $\mathtt{ObstacleFree}(q_{\text{nearest}}, q_{\text{new}})$ **then**
7       $q_{\text{min}} \leftarrow q_{\text{nearest}}$
8       $Q_{\text{near}} \leftarrow \mathtt{Near}(q_{\text{new}}, G)$
9       $\mathtt{AddVertex}(G, q_{\text{new}})$
10   **foreach** $q_{\text{near}} \in Q_{\text{near}}$ **do**
11         $c' \leftarrow \mathtt{Cost}(q_{\text{near}}, q_{\text{new}}) + \mathtt{Cost}(q_{\text{near}})$
12   **if** $c' < \mathtt{Cost}(q_{\text{near}})$ **then**
13           $q_{\text{min}} \leftarrow q_{\text{near}}$
14       $\mathtt{AddEdge}(G, q_{\text{min}}, q_{\text{new}})$
15   **foreach** $q_{\text{near}} \in Q_{\text{near}} \setminus \{q_{\text{min}}\}$ **do**
16   **if**
          $\mathtt{ObstacleFree}(q_{\text{new}}, q_{\text{near}})$ and $\mathtt{Cost}(q_{\text{near}}) > \mathtt{Cost}(q_{\text{new}}) + \mathtt{Cost}(q_{\text{new}}, q_{\text{near}})$
          then
17           $q_{\text{parent}} \leftarrow \mathtt{Parent}(q_{\text{near}})$
18           $\mathtt{RemoveEdge}(G, q_{\text{parent}}, q_{\text{near}})$
19           $\mathtt{AddEdge}(G, q_{\text{new}}, q_{\text{near}})$

The RRT* algorithm is a powerful method for searching a state-space for a feasible (or even asymptotically optimal) solution regarding motion constraints; however, some modified versions of RRT* have been developed. For example, [Kuffner and LaValle, 2000] developed a so-called RRT-Connect. It connects the furthermost extrapolation of the new sample, covering

the whole space at all time. This serves as a greedy heuristic providing faster solutions and covers uniformly the whole space. Another modification is called RRT$^\text{X}$ proposed by [Otte and Frazzoli, 2016] which is intended for a path planning in environments with dynamic obstacles. It provides constant and the fastest information propagation time keeping the tree as up to date as possible.

2.4 Fixed-Wing Aircraft Emergency Landings

If the total loss of thrust occurs, the aircraft became a glider. It needs to maintain the correct speed to minimize the sink ratio, but still, the aircraft remains controllable. [Eng, 2011] studies an emergency landing trajectory planning based on procedures adopted from manned emergency landing strategies stated in [CASA, 2007]. Author's aim is to have a single-query planning algorithm providing the final trajectory which is then followed by the aircraft. The landing path is generated such that it follows several major waypoints around the airport. The author takes wind into account, but he states that if the aircraft does not have enough altitude or if something unexpected happens, the aircraft might not be able to land. Another drawback of his proposed algorithms is they do not take obstacles nor terrain collisions into account. On the other hand, the proposed methods have been successfully deployed on a small fixed-wing UAV.

Authors of [Shapira and Ben-Asher, 2005] propose to use an excess speed for the range extension in case of the total loss of thrust. They propose a maneuver which changes the excess speed into height, and thus it extends the aircraft range.

The problem of optimal glide path planning between two points in 3D space is studied in [Adler et al., 2012]. The authors propose to use maneuvers consisting of several segments: turns, straight segments, and straight segments used for changing the aircraft speed. They propose to glide along straight segments with the optimal glide speed and to turn with different one. They use a grid discretization of the state-space for the path planing with obstacles.

2.5 Rotary-Wing Emergency Landings

The total loss of thrust on a rotary-wing aircraft is very dangerous, poses the aircraft and its crew into a huge danger because rotary-wing aircraft are not capable of good gliding. However, emergency landing with such an aircraft is still possible, but it requires special maneuvers, so-called flares.

[Choudhury et al., 2013] propose the use of RRT*-based algorithm capable of trajectory planning towards several landing sites simultaneously. Moreover, the final trajectory satisfies the aircraft motion constraints and also includes rotary-wing aircraft specific landing maneuvers. They also propose to reuse the tree by an iterative rewiring of the existing tree to the actual aircraft position making it a root allowing better planning over time. An use of the RRT* for collision free waypoints in 3D cluttered environments followed by a path smoothing for satisfying motion constraints is proposed in [Yang and Sukkarieh, 2008].

Problem Statement

Landing an aircraft without a thrust is a challenge because any mistake can be fatal. If the loss of thrust occurs, it is crucial to choose the most suitable landing site and the safest landing trajectory towards it. The decision is time-critical as the aircraft is losing the altitude and can end up in a situation that any landing site is not reachable anymore. The selected trajectory provides the pilot with enough time and terrain distance for a safe landing by maximizing the minimum height above a terrain. Such a trajectory does not end at the selected landing site but directly above it because losing an excess height is much safer, faster, and easier if it is needed than flying closely to a terrain. Moreover, it gives the pilot the best chance to solve any other unexpected issues, such as bad weather conditions.
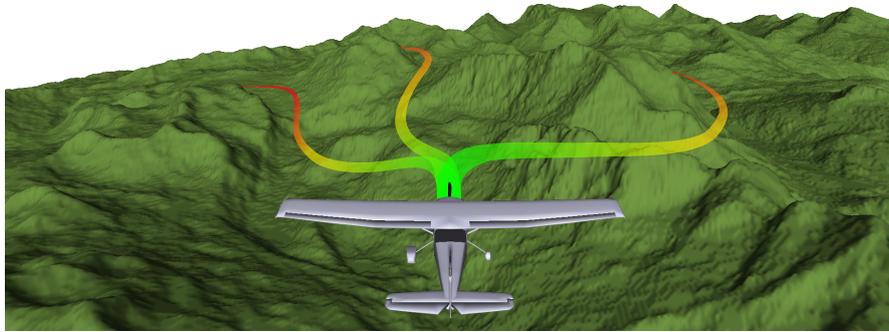
Figure 3.1: A visualization of the problem which stands for choosing the safest landing trajectory and selecting the landing site from all possibilities for an emergency landing in a case of engine failure.

We need to know the aircraft behavior and to describe it to plan the best landing trajectory. A flying aircraft can be described by its configuration $q = (x, y, z, \psi, \theta, \varphi, v)$, where (x, y, z) gives its position in the 3D space, ψ stands for its heading angle, θ gives its pitch angle, φ describes the roll angle, and v is the aircraft forward speed. Hence, the aircraft state q is from a seven-dimensional configuration space $\mathcal{C} = \mathbb{R}^4 \times \mathbb{S}^3$. An aircraft motion is constrained by the minimum turning radius and the limited pitch angle whose limits are influenced by the thrust of the motor and the trajectory curvature to maintain the aircraft speed v.

Let Ξ be a set of n lading sites $\Xi = \{\xi_1, \ldots, \xi_n\}$ with each landing site ξ_i given by the aircraft expected final configuration q^{ξ_i}. Let Γ be the emergency landing trajectory

$\Gamma : [0,1] \to \mathcal{C}$ starting at the aircraft current configuration q_{act}, i.e., $\Gamma(0) = q_{\text{act}}$. The end of the trajectory Γ is chosen from a set $\widehat{\xi}_*$ containing all configurations above the selected landing site $\xi_* \in \Xi$, i.e., $\Gamma(1) \in \widehat{\xi}_*$. Any configuration $q \in \widehat{\xi}_*$ is equal to the final configuration q^{ξ_*} of the selected landing site ξ_* except the aircraft altitude.
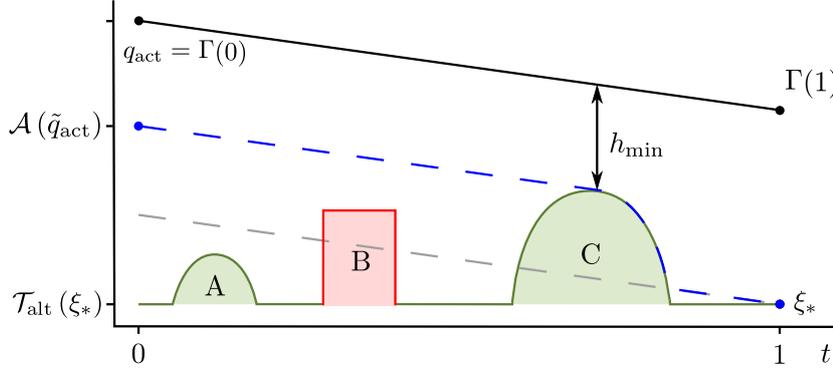

Figure 3.2: An example of the optimization criteria h_{min} for the trajectory Γ. The safety of the glide landing trajectory (the black line) is maximized by maximizing the aircraft minimum height above the terrain. In the visualized case, the value of h_{min} is influenced by the hill C with the blue dashed line representing the minimum needed altitude $\mathcal{A}$ for a safe landing. The obstacle B would influence h_{min} if the hill C is not present and the hill A can never limit the landing at ξ_* as the gray dashed line showing the minimum needed altitude for a glide with omitted obstacles and terrain indicates.

Let $\mathcal{T}_{\text{alt}} : \mathbb{R}^2 \to \mathbb{R}$ be the **aircraft minimum altitude** at a position (x,y) such that it does not collide with a terrain nor any obstacle. Then, the **aircraft minimum height above terrain** h_{min} along the trajectory Γ can be expressed as

$$h_{\text{min}} = \min_{t \in [0,1]} \Gamma_z(t) - \mathcal{T}_{\text{alt}}(\Gamma_{2\text{D}}(t)), \tag{3.1}$$

where $\Gamma_z(t)$ stands for the altitude z and $\Gamma_{2\text{D}}(t)$ stands for the aircraft 2D position (x,y) at t. The safest landing trajectory is the one which maximizes h_{min}. Therefore, the problem of selecting the best landing site ξ_* and the emergency landing trajectory Γ can be formulated as a problem of maximization of the minimum aircraft height above a terrain or obstacles

Problem 1 (Planning Safe Emergency Landing)

$$\max_{\Gamma, \xi_* \in \Xi} \quad h_{\text{min}}(\Gamma), \tag{3.2}$$

$$\text{s.t.} \quad \Gamma(0) = q_{\text{act}}, \ \Gamma(1) \in \widehat{\xi}_*. \tag{3.3}$$

Therefore, we are looking for a landing site ξ_* and landing trajectory Γ maximizing (3.1). An example of h_{min} is shown in Fig. 3.2 whereas Fig. 3.1 shows an example of the determination of the landing site and emergency landing trajectory in general.

The crucial part of the emergency landing trajectory planning is a model of an altitude loss for the specified 2D trajectory of the particular aircraft. The altitude loss, i.e., the altitude difference between two aircraft configurations is defined by the following equation for $t_1, t_2 \in [0,1], t_1 < t_2$

$$\mathcal{H}(\Gamma(t_1), \Gamma(t_2)) = \Gamma_z(t_1) - \Gamma_z(t_2), \tag{3.4}$$

where $\mathcal{H}$ is the **altitude loss function**. The particular altitude loss function is described in Chap. 4, where the optimization of turning radii is considered to achieve the lowest altitude loss for fixed-wing aircraft.

Model of a Gliding Aircraft and Its Altitude Loss Function

When the total loss of thrust occurs, the pilot needs to preserve as much altitude as possible, i.e., to optimize the altitude loss. As [FAA, 2016] suggests, it is wise to maintain the best glide speed during a forced landing after the total loss of thrust. The altitude loss optimization can be achieved by maintaining the optimal glide speed and optimizing the utilized turning radii. A proper model of the aircraft glide and altitude loss is needed to plan such an optimized trajectory.

4.1 Dynamic Model of an Aircraft

Aircraft dynamics is influenced mainly by four forces – lift $\mathbf{L}$, drag $\mathbf{D}$, thrust $\mathbf{T}$ and weight $\mathbf{W}$, see Fig. 4.1. An aircraft is flying straight without accelerating, i.e., it does not turn nor change its speed, during a normal steady flight. In such conditions, all acting forces cancel out, and the resultant force is equal to zero. If the aircraft turns but still maintains its speed, the resultant force of these four acting forces causes a centripetal acceleration, i.e., the aircraft turning.
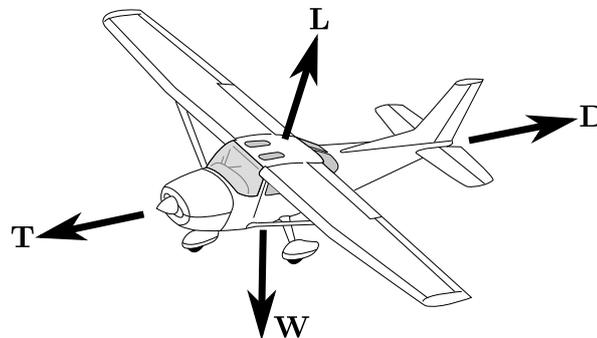

Figure 4.1: Forces acting on an aircraft. Both thrust $\mathbf{T}$ and drag $\mathbf{D}$ act in parallel with the direction of flight, weight $\mathbf{W}$ acts vertically and lift $\mathbf{L}$ is perpendicular to the wing plane.

As described in [Beard and McLain, 2012], assuming the aircraft flies in a standard flight envelope, the magnitudes of the lift and drag are influenced by the lift coefficient C_{L} and drag coefficient C_{D}

$$L = \|\mathbf{L}\| = \frac{1}{2}\rho C_{\mathrm{L}} S v^2\,, \quad D = \|\mathbf{D}\| = \frac{1}{2}\rho C_{\mathrm{D}} S v^2\,, \tag{4.1}$$

where S is the wing area, ρ is the air density, and v is the aircraft speed. The drag consists of two components; the geometric drag, which is constant and it is given mainly by the aircraft body, and the lift-induced drag, which is dependent on the actual lift. Hence, as [Roskam, 1985, Durham, 2013] suggest, the drag can be expressed as

$$C_{\mathrm{D}} = C_{\mathrm{D}0} + k C_{\mathrm{L}}^2\,, \tag{4.2}$$

where $C_{\mathrm{D}0}$ is the coefficient of the geometric drag, also known as the zero-lift drag coefficient, and k is the lift-induced drag coefficient. It is influenced by the wing area S, the wingspan b and the span efficiency factor ϵ. The value of k can be expressed as

$$k = \frac{S}{\pi b^2 \epsilon}\,. \tag{4.3}$$

All the above coefficients are different for each aircraft type, and they vary significantly with its size. In our work, we focus on one of the most common general aviation aircraft Cessna 172 whose numerical values of these coefficients can be found in Tab. 5.1.

A configuration of an aircraft is given by its position (x, y, z), heading angle ψ, pitch angle θ, and roll angle φ. Two simplifications are made to have a model with a closed-form solution. First, the pitch angle is equivalent to the angle of descent, i.e., the angle of attack is zero, but still, the model is very similar to the full dynamic model of a steady flight. Secondly, the flight is expected to be smooth and controlled. Moreover, we assume the aircraft flies exactly in the direction of its orientation, i.e., the sideslip is zero as well. Thus, the yaw angle is equivalent to the heading angle ψ. As a consequence of these simplifications, the bank angle is identical to the roll angle φ. Such a simplified model can be expressed as

$$\dot{x} = v \cos\psi \cos\theta\,, \tag{4.4}$$
$$\dot{y} = v \sin\psi \cos\theta\,, \tag{4.5}$$
$$\dot{z} = v \sin\theta\,, \tag{4.6}$$
$$\dot{v} = \frac{1}{m}(T - D - W \sin\theta)\,, \tag{4.7}$$
$$\dot{\psi} = \frac{L \sin\varphi}{mv}\,, \tag{4.8}$$

where m is the aircraft mass, $T = \|\mathbf{T}\|$, $W = \|\mathbf{W}\| = mg$, and g is the gravitational acceleration.

4.2 Model of a Gliding Aircraft

In a case of emergency landing without a thrust, the steady descending flight is considered to the best choice [McClamroch, 2011, FAA, 2016]. Let's assume the flight trajectory is divided into several segments with fixed turning radii, e.g., Dubins maneuver. Then, the pitch and

roll angles are constant along each trajectory segment. Although this model allows disconti-nuities in the pitch and roll angles between segments, those discontinuities are a reasonable simplification. First, changes of the roll angle are very fast with a significantly lesser time constant than the pitch angle. Secondly, even though the time constant of the pitch angle is not negligible, the aim is to preserve the maximum possible pitch angle. Hence, pitch angle changes are expected to be small enough for making this simplification reasonable. On top of that, the aircraft vertical acceleration $\ddot{z}$ is assumed to be zero which strictly enforces the lift to counterweight the gravitational force, and thus

$$L \cos \varphi \cos \theta = W \,. \tag{4.9}$$

The constant speed and a loss of thrust enforce the lift to counterweight the drag force as well, and so

$$L \cos \varphi \sin \theta = D \,. \tag{4.10}$$

Moreover, the change of the aircraft heading can be described by

$$\dot{\psi} = \frac{v \cos \theta}{R} \,. \tag{4.11}$$

By the combination of equations (4.8), (4.11) and substituting L from (4.9), we get

$$\frac{W \sin \varphi}{mv \cos \varphi \cos \theta} = \frac{v \cos \theta}{R} \,. \tag{4.12}$$

The aircraft is assumed to be flying with the optimal gliding speed to lose the least possible altitude per flown distance. Therefore, the pitch angle is small ($\theta < 0$) clearing the way for assuming $\cos \theta \approx 1$. As shown in Fig. 4.2, the introduced errors by this simplification are much smaller than 5% and do not significantly affect the model. If more accurate results are needed, numerical methods for solving (4.12) have to be used. However, for the used approximation and knowing $W = mg$, the roll angle can be approximated from (4.12) as

$$\varphi \approx \tan^{-1} \left(\frac{v^2}{Rg} \right) \,. \tag{4.13}$$

The lift coefficient needed for the steady flight is determined from (4.1) and (4.9) giving us

$$C_{\mathrm{L}} = \frac{2W}{\rho S v^2 \cos \varphi \cos \theta} \,. \tag{4.14}$$

Substituting the roll angle from (4.13), we get

$$C_{\mathrm{L}}(R) = \frac{2W \sqrt{\left(\frac{v^2}{Rg} \right)^2 + 1}}{\rho S v^2 \cos \theta} = \frac{H(R)}{\cos \theta} \,, \tag{4.15}$$

where $H(R)$ is considered to be constant for a constant speed v, fixed turning radius R, and constant aircraft mass m. Using (4.2), the drag coefficient can be expressed in terms of the pitch angle and turning radius as

$$C_{\mathrm{D}}(R) = C_{\mathrm{D}0} + k \frac{H^2(R)}{\cos^2 \theta} \,. \tag{4.16}$$
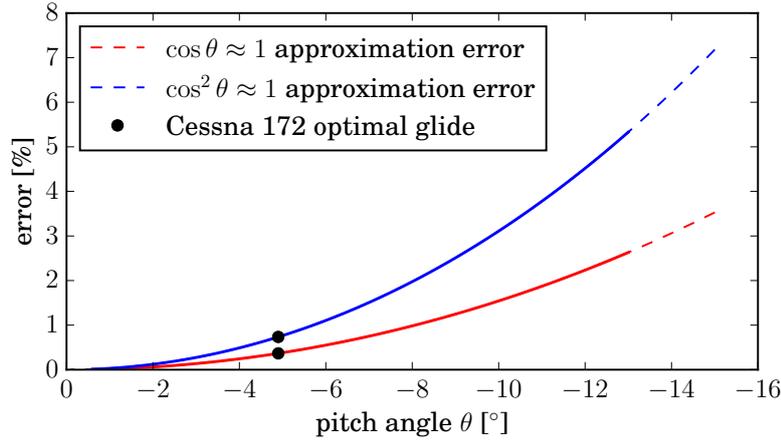
Figure 4.2: Errors introduced by considered approximations $\cos\theta \approx 1$ and $\cos^2\theta \approx 1$ are shown by dashed lines. The pitch angle for the optimal glide is dependent on the aircraft type and generally it is in a range $-0.5°$ and $-10°$. Corresponding errors are shown by solid lines and the errors for Cessna 172 optimal glide are highlighted.

The aircraft speed is considered to be constant ($\dot{v} = 0$) and the thrust is not available after the engine malfunction ($T = 0$), and thus using (4.7), the drag must be compensated by the altitude loss

$$D + W\sin\theta = 0 \tag{4.17}$$

which can be expressed using (4.1) and (4.16) as

$$\left(C_{\mathrm{D0}} + k\frac{H^2(R)}{\cos^2\theta}\right) = -\frac{2W\sin\theta}{\rho Sv^2}. \tag{4.18}$$

Finally, the pitch angle is small; so, the approximation $\cos^2\theta \approx 1$ can be used. It introduces only errors smaller than 6% (see Fig. 4.2) and so, the closed-form solution for the pitch angle depending on the turning radius can be found as

$$\theta(R) \approx -\sin^{-1}\left(\frac{\rho Sv^2\left(C_{\mathrm{D0}} + kH^2(R)\right)}{2W}\right), \qquad H(R) = \frac{2W\sqrt{\left(\frac{v^2}{Rg}\right)^2 + 1}}{\rho Sv^2}. \tag{4.19}$$

The curvature κ of the trajectory can be computed as

$$\kappa = \frac{|x'y'' - y'x''|}{(x'^2 + y'^2)^{\frac{3}{2}}}, \tag{4.20}$$

and the relation between the curvature κ and turning radius R is

$$\kappa = \frac{1}{R}. \tag{4.21}$$

Then, the closed-form solution for the pitch angle given by the trajectory curvature is given by

$$\theta(\kappa) \approx -\sin^{-1}\left(\frac{\rho S v^2 \left(C_{\mathrm{D0}} + kH^2(\kappa)\right)}{2W}\right), \qquad H(\kappa) = \frac{2W\sqrt{\left(\frac{\kappa v^2}{g}\right)^2 + 1}}{\rho S v^2}. \tag{4.22}$$

4.3 Altitude Loss Function

When the aircraft loss the thrust totally, it becomes a glider. From that moment, it loses its altitude without a chance to gain it. Knowing how the aircraft loses an altitude is a key factor for planning a safe emergency landing trajectory.

Let $\Gamma : [0,1] \to \mathcal{C}$ be a trajectory between aircraft configurations q_1 and q_2, i.e., $\Gamma(0) = q_1$ and $\Gamma(1) = q_2$. Since the goal is to optimize the altitude loss, the pilot can directly influence only the turning radius and the aircraft heading angle. Thus, the vertical profile of the trajectory Γ is determined by its 2D projection $\Gamma_{\mathrm{2D}} : [0,1] \to \mathbb{R}^2$, i.e., $\Gamma_{\mathrm{2D}}(0) = q_1^{\mathrm{2D}}$ and $\Gamma_{\mathrm{2D}}(1) = q_2^{\mathrm{2D}}$, where q_1^{2D} and q_2^{2D} are 2D projections of q_1 and q_2, respectively. The trajectory projection can be described by its curvature $\kappa(t)$. Having the closed-form solution (4.22) for the pitch angle given by the trajectory curvature, the **altitude loss function** $\mathcal{H}$ between q_1^{2D} and q_2^{2D} can be described as

$$\mathcal{H}\left(q_1^{\mathrm{2D}}, q_2^{\mathrm{2D}}\right) = \int\limits_0^1 -\sin\theta(\kappa(t))\|\Gamma_{\mathrm{2D}}{}'(t)\|\,\mathrm{d}t, \tag{4.23}$$

where $\|\Gamma_{\mathrm{2D}}{}'(t)\|$ gives the magnitude of the spatial derivative of the 2D projection of the trajectory Γ at the relative distance t.

4.3.1 3D Trajectory Generation and Turning Radius Optimization

The altitude loss function (4.23) describes the altitude loss along a 2D projection of any arbitrary trajectory. However, it involves integration, which enforces a use of numerical solvers. Few assumptions have to be made to have a closed-form solution.

First, we can assume the projected trajectory can be divided into n segments with a constant curvature $\kappa_i \in [0, \kappa_{\max}]$ along each segment. Then, the altitude loss function along such a trajectory can be expressed by

$$\mathcal{H}\left(\kappa_1, \kappa_2, \ldots, \kappa_n\right) = \sum_1^n -\mathcal{L}_i \tan(\theta(\kappa_i)), \tag{4.24}$$

where $\mathcal{L}_i$ is the 2D length of the i-th segment and κ_i is its curvature. Without loss of generality, we can assume the trajectory can be divided into only three segments allowing to simplify the altitude loss function into

$$\mathcal{H}\left(\kappa_1, \kappa_2, \kappa_3\right) = \sum_1^3 -\mathcal{L}_i \tan(\theta(\kappa_i)). \tag{4.25}$$

The most known three-segment curvature-constant trajectory in a plane is Dubins maneuver, firstly described in [Dubins, 1957]. Such a maneuver consists of three circular segments

with the maximum curvature or with the maximum curvature along the first and third segment and zero curvature along the second segment, see Fig. 2.1. A Dubins maneuver is the shortest possible curvature-constrained maneuver in a plane connecting two points with prescribed heading angles. Nevertheless, the shortest maneuver is not the optimal one in terms of the altitude loss (4.25). [Chaudhari et al., 2014] showed that Dubins maneuver with different curvatures along each segment has a closed-form solution as well. Thus, we can get a closed-form solution for such a trajectory. Moreover, we can define the optimization of the altitude loss along such a trajectory as

$$\min_{\kappa_1,\kappa_2,\kappa_3} \quad \mathcal{H}(\kappa_1, \kappa_2, \kappa_3) \,. \tag{4.26}$$

From (4.22) it is clear that the larger curvature is used, the higher altitude loss is. If the middle segment of the maneuver is the circle, i.e., $\kappa_2 > 0$, the lost altitude along this segment is definitely higher than the altitude loss along a straight segment. Moreover, making the middle segment a circle cannot shorten the maneuver, unless the connected points are closer than $4R_{\min}$. Aircraft usually fly over long distances so we can assume the middle segment is a straight segment, i.e., $\kappa_2 = 0$. It allows us to further reduce one degree of freedom during the optimization which can be then expressed as

$$\min_{\kappa_1,\kappa_3} \quad \mathcal{H}(\kappa_1, 0, \kappa_3) \,. \tag{4.27}$$

An example of this optimization is depicted in Fig. 4.3.

**(a)** Maneuvers   **(b)** Altitude loss
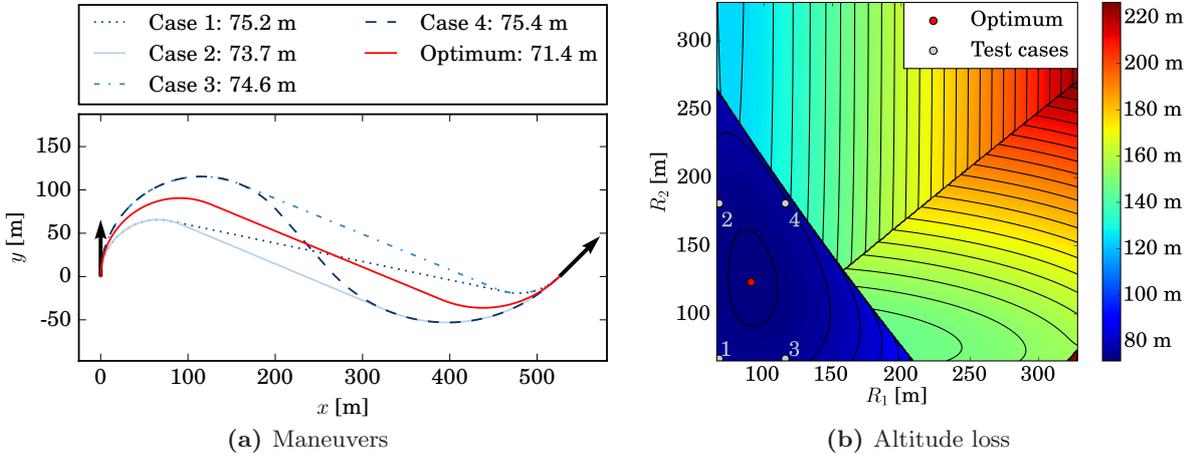
Figure 4.3: Examples of CSC Dubins maneuvers for Cessna 172 with different radii connecting two points with prescribed heading angles are presented in (a) whereas corresponding altitude losses for different turning radii are shown in (b). Five maneuvers with different turning radii are shown. The maneuver with the minimum altitude loss is shown by the solid red line.

Model Evaluation for Cessna 172

In this work, we propose a novel emergency landing path planning algorithm for fixed-wing aircraft. We have decided to use one of the most popular general aviation aircraft for an evaluation of the real behavior of the proposed approach. Here, we study the performance of a gliding aircraft model for this particular aircraft. According to [Turnbull, 1999], about 13.5% of general aviation aircraft are from Cessna 172 family. Another 13.3% of the market is made by Paper PA28 family, which is very similar to the Cessna 172 family. Hence, we have chosen Cessna 172 as a model for the evaluation of the proposed method. Its parameters are summarized in Tab. 5.1.

Table 5.1: Technical parameters of Cessna 172.

Parameter	Symbol	Value
Vehicle mass[1]	m	1,000 kg
Wing area	S	16.2 m^2
Wingspan	b	11 m
Span efficiency factor	ϵ	0.8
Coefficient of geometric drag	C_{D0}	0.0341
Optimal glide airspeed	v	33.4 m·s^{-1}
Lift-induced drag coef.	k	0.053
Maximum roll angle	$|\varphi_{max}|$	60°
Minimum turning radius	R_{min}	65.7 m
Maximum gliding pitch angle	θ^g_{max}	−4.9°
Minimum gliding pitch angle	θ^g_{min}	−13.1°

5.1 Altitude Loss for Cessna 172

An accurate model of the altitude loss is a key factor for the accurate emergency landing path planning. The model of a gliding aircraft is described in Chap. 4 and its parameters

---

[1]The mass of Cessna 172 varies from 767 kg when empty to 1,111 kg when fully loaded.

need to be known for a numerical altitude loss determination. The used parameters for Cessna 172 are depicted in Tab. 5.1. Having these parameters, the pitch θ and roll φ angles can be calculated from (4.13) and (4.19) for various turning radii R. Computed values are depicted in Fig. 5.1 where the minimum turning radius is $R_{\min} \approx 65.7$ m corresponding to the maximum roll angle of $|\varphi_{\max}| = 60°$. The aircraft experiences the steepest descent (the minimum pitch angle) during such a turn with the pitch angle of $\theta^g_{\min} \approx -13.1°$. In contrary, the shallowest descent (the maximum pitch angle) is achieved for a straight flight during which the pitch angle is only $\theta^g_{\max} \approx -4.9°$. Therefore, the minimum possible altitude loss is achieved by a straight flight during which the aircraft loses 85.7 meters per flown kilometer and the maximum possible altitude loss during a steady turning maneuver with the optimal glide speed is 232.7 meters per flown kilometer for a turn with the minimum turning radius. This demonstrates the pilot's ability to quickly lose excess altitude by making S-shaped turns when needed. Moreover, other techniques such as a forwardslip can be used for losing excess altitude.


(a) Roll and pitch angles

(b) Altitude loss in lost meters per flown kilometer
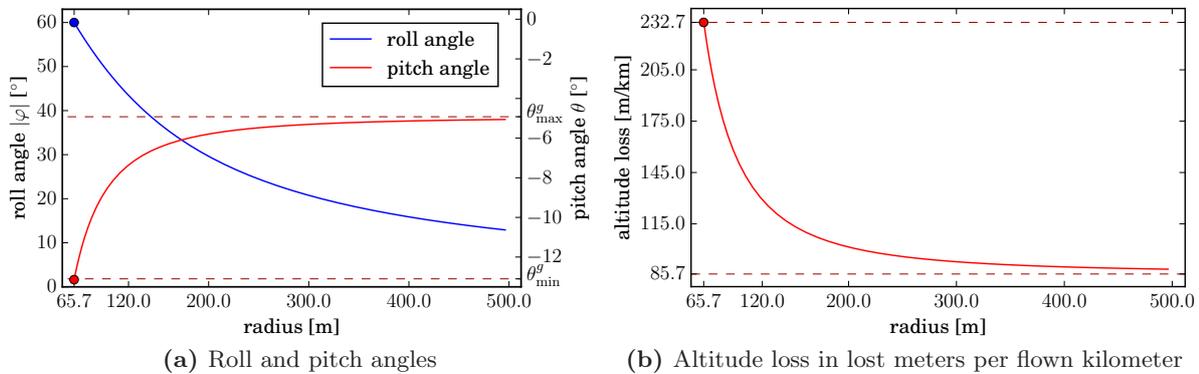
Figure 5.1: The pitch and roll angles and altitude loss as a function of the selected turning radius R for Cessna 172 during a gliding. The values are computed using (4.13) and (4.19) with the parameters of Cessna 172 depicted in Tab. 5.1.

5.1.1   Model Comparison

Authors of [Paul et al., 2017] describe a model of Cessna 172 and its glide ratio and bank angle based on the turning radius. To compare our model deduced in Chap. 4 with their work, we have computed the roll angle and glide ratio from (4.13) and (4.19) for turning radii stated in their work. The achieved results are depicted in Tab. 5.2.

Table 5.2: A comparison of models of gliding Cessna 172

	R [m]	65.8	114.0	197.5	313.3	646.8	∞
Model of Cessna 172	ψ	60°	45°	30°	20°	10°	0°
[Paul et al., 2017]	Glide ratio	4.5:1	6.36:1	7.79:1	8.45:1	8.61:1	9:1
Proposed model	ψ	60°	45°	30°	20°	10°	0°
	Glide ratio	4.30:1	7.47:1	9.82:1	10.83:1	11.43:1	11.63:1

Data for the model of Cessna 172 in [Paul et al., 2017] were computed for the optimal glide speed of 65 kts. We assume the same optimal glide speed in our model. Moreover, this

same speed is proposed in [FAA, 2016] as well. We can see that our model provides better gliding ratios. Other parameters than the airspeed of the model from [Paul et al., 2017] are not stated, and therefore, we are not able to compare these two models with the same parametrization. Thus, we assume differences are caused only by using different parameters.

5.2 Maneuver Turning Radii Optimization

The pilot directly influences only the roll angle (turning radius) and the heading angle during the optimal glide. Therefore, we plan the 2D projection of the trajectory and we determine its vertical profile from the altitude loss function (4.23). In our case, we use the CSC type of Dubins maneuver for the generation of the projected trajectory and optimize its vertical profile according to the modified version of the altitude loss function (4.25) Nevertheless, the two-dimensional optimization (4.27) optimizes the used turning radii on the interval $R_i \in [R_{\min}, \infty)$. Thus, it is computationally intractable in a finite time with a dense sampling. Therefore, we propose further simplification to make the planning problem computational tractable and to provide real-time information about the safest trajectory to the pilots.

5.2.1 Upper Limit for the Radii Optimization

We have decided to analyze behavior of the radii optimization and to set up a proper upper limit $R_{\max}$, and make the radii optimization computationally feasible. Thus, the optimization would take place on the interval $R_i \in [R_{\min}, R_{\max}]$ instead of $R_i \in [R_{\min}, \infty)$.

Figure 5.2: Scheme of a setup with $\psi_{\text{start}} = 30°$ and $\psi_{\text{end}} = 90°$.

Let's have two points $p_{\text{start}} = (0,0)$ and $p_{\text{end}} = (0,l)$ with prescribed heading angles $\psi_{\text{start}}, \psi_{\text{end}} \in \{0°, 10°, \dots, 350°\}$ and $l \in \{300, 400, \dots, 3000\}$ m. An example of such a scenario can be found in Fig. 5.2. For every setup, the optimal maneuver is found by constructing the CSC Dubins maneuver and its optimization (4.27). To make the optimization computable (but still very demanding), every maneuver is optimized on the interval $R_i \in [R_{\min}, 5l]$ because the altitude savings for the very long turning radii are expected to be very small and negligible.

All turns have been processed and results are depicted in Fig. 5.3. We can clearly see, that the most of occurring turns in the optimal maneuvers have smaller turning radius $R_i \leq 5R_{\min}$. In fact, 14.5% of turns use a longer turning radius $R_i > 5R_{\min}$. On the other hand, those turns are usually small and save only small amount of altitude. Thus, we have decided to limit the radii optimization (4.27) by $R_i \in [R_{\min}, 5R_{\min}]$ to make it computationally tractable. Moreover, the affection of the optimal altitude loss is negligible.

5.2.2 Performance of the Radii Optimization

We have also prepared an experiment to evaluate results of the radii optimization. Similarly to the previous setup, let's have two points $p_{\text{start}} = (0,0)$ and $p_{\text{end}} = (0,l)$ with the prescribed heading angles $\psi_{\text{start}}, \psi_{\text{end}} \in \{0°, 10°, \dots, 350°\}$ and $l \in \{300, 550, 1000, 2500\}$ m. The CSC

(a) Distance $l \in \{300, 400, \ldots, 1000\}$ m   **(b)** Distance $l \in \{1100, 1200, \ldots, 3000\}$ m
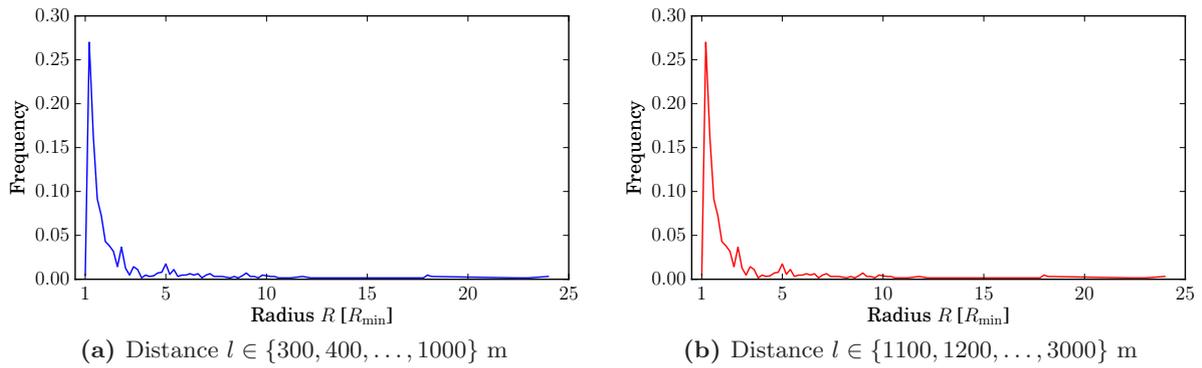
Figure 5.3: Frequency of a turn with the radius R determined by all optimized maneuvers between the points separated by the distance l and with all headings $\psi_{\text{start}}, \psi_{\text{end}} \in \{0°, 10°, 20°, \ldots, 350°\}$. Turns with a turning angle smaller than $5°$ have been omitted.

Dubins maneuver using the minimum turning radius is created for each such a scenario. Then, the maneuver is optimized on $R_i \in [R_{\text{min}}, 5R_{\text{min}}]$ according to (4.27).

Three properties are studied on the optimized maneuvers. First, the relative savings of the optimal maneuver to the maneuver using the minimum turning radius are studied. Secondly, the relative cost to the theoretical minimum altitude loss $\mathcal{H}_{\text{min}}$ on the distance l

$$\mathcal{H}_{\text{min}} = -l \tan \theta^g_{\text{min}} \tag{5.1}$$

is studied. The theoretical minimum altitude loss corresponds to the altitude loss along the straight trajectory of a length l, i.e., the effect of a proper path planning is studied. Finally, the ratio of the turn lengths to the whole maneuver is studied. The results are depicted in Fig. 5.4.

5.2.3   Model Evaluation

Results depicted in Fig. 5.4 show it is possible to save up to 20% of the altitude loss by the proposed radii optimization (4.27) in comparison to maneuvers using the minimum turning radius. Moreover, if the trajectory is not planned well, it can be up to 4.5 times more expensive only by choosing inappropriate heading angles. The results also show that longer distances between points cause the lower relative savings. Nevertheless, the absolute savings are nearly independent on the distance between points.

As a conclusion, the proposed turning radii optimization (4.27) can be considered as the global optimization function for planning in a free space. Hence, the found maneuver provides the safest trajectory to the selected landing site. In dense spaces with a lot of obstacles and/or difficult terrain, the proposed optimization should be considered as a local optimization function for a trajectory between two points. The whole trajectory towards the selected landing site can be built up by using randomized algorithms for state-space searching, such as the RRT*.
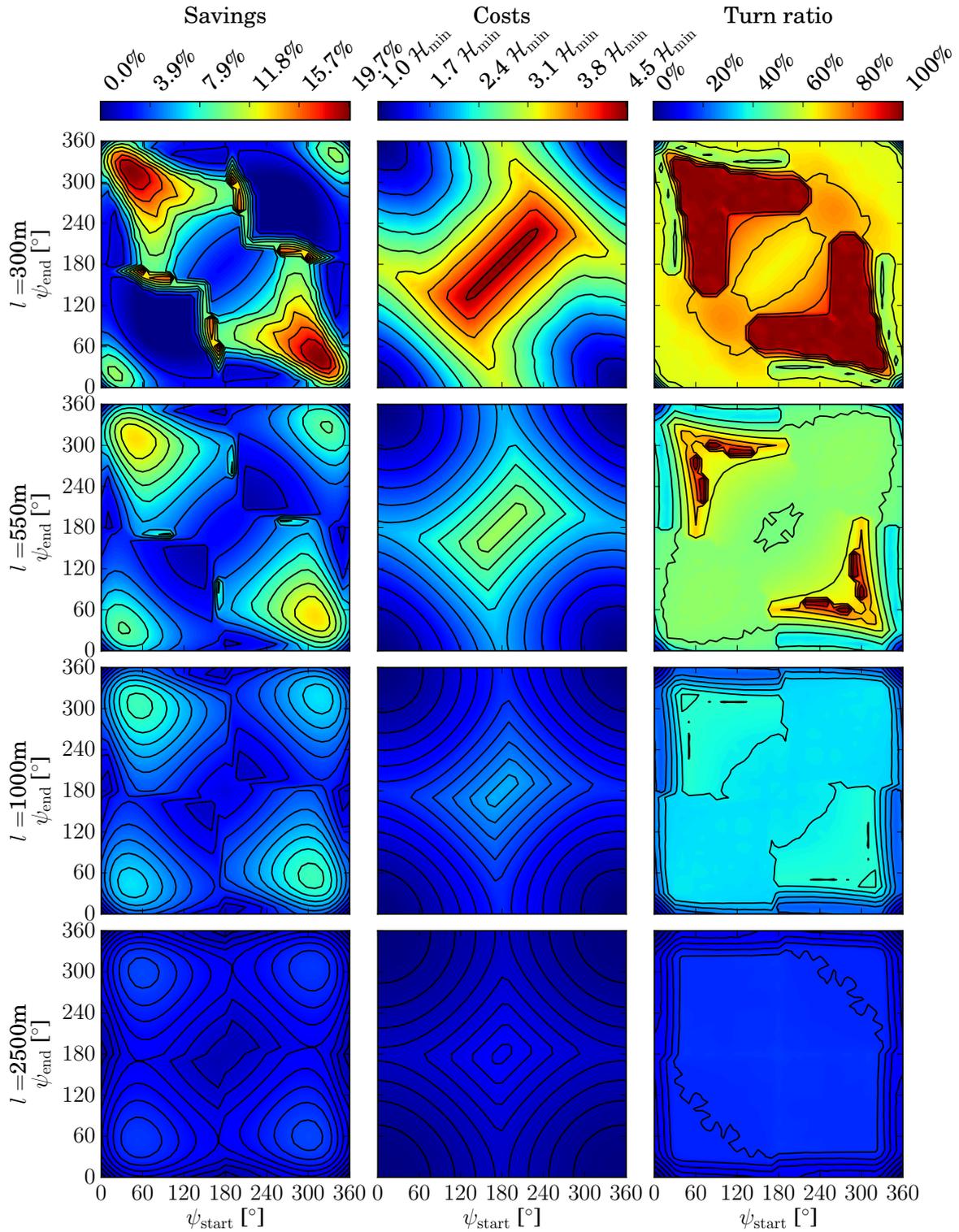
Figure 5.4: Results of the radii optimization on a single CSC maneuver between the points $p_{\text{start}} = (0,0)$ and $p_{\text{end}} = (0,l)$ with the heading angles $\psi_{\text{start}}, \psi_{\text{end}} \in \{0°, 10°, 20°, \ldots, 350°\}$. All possible CSC maneuvers, such that $R_1, R_3 \in \{1, 1.1, \ldots, 5\} R_{\text{min}}$, between these two configurations are examined and the one with the minimum possible altitude loss is chosen as the optimal one. Left plots show the saved altitude regarding Dubins maneuver utilizing the minimum turning radius R_{min}, middle plots show the altitude loss relative to the theoretical minimum $\mathcal{H}_{\text{min}}$ (5.1) (straight flight) and the right ones show the relative length of turns to the length of the maneuver.

Proposed Informed RRT*-based Method

In case of the loss of thrust, the pilot is requested to find the most suitable landing site and a feasible emergency landing trajectory towards it. The Problem 1 with its optimization criteria (3.2) stands to choose a landing site and a landing trajectory providing the highest margin to the terrain and obstacles along the whole landing trajectory. After the total loss of thrust, the aircraft glides and loses its altitude making this problem challenging. Moreover, the decision about the landing site and trajectory has to be made as quickly as possible. Otherwise, the aircraft can get into a situation that any landing site is not reachable anymore.

6.1   Key Properties of the Proposed Method

The Problem 1 of an emergency landing planning stand for choosing the safest landing site and an emergency landing trajectory towards it. The task is to maximize the minimum height above the terrain and obstacles raising the following issues:

1. An emergency landing path starts at the actual configuration of the aircraft.

2. Consider multiple landing sites simultaneously.

3. Satisfy the motion constraints of the aircraft.

Moreover, we extend these raised issues to describe the required properties of the proposed method; to have a fast, reliable, and high-quality solution providing algorithm:

4. Preserve the roadmap allowing movements of the aircraft during its construction.

5. Provide high-quality solutions as quickly as possible after the engine malfunction.

6. Provide a solution whenever it is needed.

To address these issues, we propose to employ a modified version of the RRT* algorithm [Karaman and Frazzoli, 2011]. The main reason why we base our proposed method on the

RRT* is fairly simple; it is a well known algorithm capable of finding a collision-free trajectories in a space of arbitrary dimension, if such a trajectory exists. Moreover, the solution improves with time. The following modifications have to be made.

6.1.1   The Dual Problem

The biggest challenge for the proposed informed RRT*-based method is to handle the aircraft movements. In a regular version of the RRT*, a root of the tree is fixed. Moving a root means the whole tree is not up-to-date, and so it have to be either updated or created again.

We consider a dual problem to the formulated Problem 1 to address this issue, and thus proposed to solve Problem 2.

Problem 2

$$\min_{\Gamma, \xi_* \in \Xi} \qquad \mathcal{A}(q_{\text{act}}), \tag{6.1}$$

$$\text{s.t.} \qquad \Gamma(0) \in \widehat{q}_{act}, \ \Gamma(1) = \xi_*, \tag{6.2}$$

where $\widehat{q}_{\text{act}}$ is a set of all configurations identical to the configuration q_{act} except the altitude. The dual problem stands to find the minimum altitude $\mathcal{A}(q_{\text{act}})$ allowing a safe landing from the actual aircraft position instead of maximizing the minimum height above a terrain h_{min} during the landing. It allows us to expand the roadmap from landing sites towards the aircraft eliminating the difficulties with aircraft movements. Moreover, it gives us the possibility of finding the emergency landing path even before the loss of thrust occurs.

6.1.2   Reduction of State-Space Dimensions

RRT*-based algorithms are computationally demanding. The demand increases with dimensions of the searched state-space. Thus, we propose a simplification to the full dynamic aircraft model described in Chap. 4, which has seven degrees of freedom. The simplified model used in the proposed modified RRT*-based algorithm omits the altitude z which is encoded in the cost of every node in the roadmap. We also omit the pitch angle θ assuming the emergency landing path to maximize the utilized pitch angle providing only small changes in it. Hence, allowing its discontinuities introduces minimal errors. Moreover, the final emergency trajectory has to be processed to deal with the excess altitude giving a possibility to solve these discontinuities. Finally, we propose to omit the roll angle φ as well. The time constants of the roll angle are in general very small, and such a discontinuity in the roll angle gives us an opportunity to employ simpler curves such as Dubins maneuvers in the proposed method making it less computationally demanding. Thus, the proposed simplified state $\tilde{q} = (x, y, \psi)$ used in the proposed method consists of the 2D position (x, y) and heading angle ψ, i.e., $\tilde{q} \in SE(2)$. As a consequence, the simplified configuration $\tilde{q}$ has only three degrees of freedom instead of seven making the proposed method faster and less computationally demanding by several orders of magnitude.

6.1.3   Collision Check and Altitude Discontinuities

The RRT* implements a collision checking function to verify that newly generated samples are collision-free. In our case, we are looking for the minimum altitude at a given configuration

allowing safe landing. The aircraft can safely land from any configuration if it has enough altitude. Thus, we propose to not use the collision detection directly in the determination of feasibility of the samples but we determine the necessary altitude modifications to keep all samples collision-free as follows.

Let $\Gamma_i : [0, 1] \to \mathcal{C}$ be the initial maneuver between two configurations. The maneuver has to be checked for collisions with the terrain and obstacles and in case the maneuver is not collision-free, it is heightened to avoid collisions. Denote $\Gamma_z(t)$ the altitude at the position t within the maneuver and $\Gamma_{2D}(t)$ as the 2D position at that point. Then, a collision is detected if the maneuver altitude is lower than the altitude of the terrain or any obstacle beneath it, i.e.,

$$\exists t : \Gamma_{i,z}(t) < \mathcal{T}_{alt}\left(\Gamma_{i,2D}(t)\right) . \tag{6.3}$$

There might be multiple collisions, and so the maximum one is determined and the whole maneuver is heightened by Δh

$$\Delta h = \max_t \left[\mathcal{T}_{alt}\left(\Gamma_{i,2D}(t)\right) - \Gamma_{i,z}(t)\right] . \tag{6.4}$$

Such a heightening causes a discontinuity at a parent node as this maneuver connects to the parent node at the altitude higher by Δh. Thus, the aircraft margin from the minimum safe altitude is further heightened by Δh after its arrival at the parent node. That makes its further flight even safer. But it also means that the aircraft has an excess altitude. The excessive altitude is considered to be safe, because we assume that any obstacle cannot be flown under. Moreover, the excess altitude can be quickly lost if desired. Thus, these altitude discontinuities in the roadmap and the excess altitude of the aircraft can be left up to the pilot or can be solved during retrieving the final landing trajectory.

6.1.4 Transformation of a Forest into a Tree

Another issue is to consider multiple landing sites simultaneously. We can grow a tree from every possible landing site making a forest of planning trees. Having several trees introduce complications, such as their penetrations, information sharing, etc.

In our case, this forest can be easily transformed into one planning tree preserving all the positive properties and eliminating the negative ones. It can be done by connecting roots, i.e., landing sites, of every tree into a virtual node. We aim to minimize the minimum altitude $\mathcal{A}\left(q_{act}\right)$ needed for a safe emergency landing. Hence, the cost of the virtual root is considered to be zero, and costs of virtual edges correspond to altitudes of the landing sites. Then, every inserted node naturally chooses its best landing site, and if better landing site is found, the node is reconnected to it during the rewiring precess needed for optimality of the algorithm.

6.2 Informed RRT*-based Method

We propose a novel RRT*-based algorithm summarized in Algorithm 3 to tackle all the mentioned issues. The algorithm is initialized by inserting nodes corresponding to all possible landing sites into a graph G and their minimum altitude $\mathcal{A}$ allowing safe landings from these points, i.e., the costs are set to the altitude of the relevant landing site ξ_i. Then, the main cycle of the roadmap expansion is started and runs until a detection of an aircraft engine malfunction, which is denoted by the `IsMotorRuning`() procedure. The proposed algorithm

is very similar to the original RRT* algorithm except the fact that we do not use the collision checking procedure during the roadmap expansion for determination of the sample feasibility. Instead, we use the collision check for the determination of the needed altitude because the aircraft can safely land from any configuration if it has enough altitude. Such a check can be done during the determination of the minimum altitude loss. We create the maneuver and if a collision is detected, the whole maneuver is heighten by the minimum possible height Δh so it does not collide. Such a maneuver guarantees a collision-free trajectory concerning the terrain and obstacles and minimizes the altitude loss and the additional altitude Δh is included in the altitude loss. Thus, the minimum altitude $\mathcal{H}(\tilde{q}_i, \tilde{q}_j)$ is considered to be lost during a flight from $\tilde{q}_i$ to $\tilde{q}_j$.

Algorithm 3: A Novel RRT*-based Algorithm for Planning Emergency Landing

Input: $\Xi = \{\xi_1, \ldots, \xi_n\}$ – the set of landing sites
Input: $\tilde{q}_{\text{act}}$ – the current position of the aircraft
Output: Γ – the best emergency landing trajectory

1 $G \leftarrow \{\boldsymbol{V} \leftarrow \Xi \cup v_{\text{virt}}, \boldsymbol{E} \leftarrow \bigcup_i^n (v_{\text{virt}}, \xi_i)\}$
2 $\mathcal{A}(\xi_i) \leftarrow \mathcal{T}_{\text{alt}}(\xi_i), \ \forall \xi_i \in \Xi$
3 **while** IsMotorRunning() **do**
4 $\quad$ $\tilde{q}_{\text{act}} \leftarrow$ UpdateAircraftConfiguration()
5 $\quad$ $\tilde{q}_{\text{rand}} \leftarrow$ SampleInformed($\Xi, \tilde{q}_{\text{act}}$)
6 $\quad$ $\tilde{q}_{\text{nearest}} \leftarrow$ Nearest($\tilde{q}_{\text{rand}}, G$)
7 $\quad$ $\tilde{q}_{\text{new}} \leftarrow$ Steer($\tilde{q}_{\text{nearest}}, \tilde{q}_{\text{rand}}$)
8 $\quad$ $Q_{\text{near}} \leftarrow$ Near($\tilde{q}_{\text{new}}, G$)
9 $\quad$ $\tilde{q}_* \leftarrow \arg\min_{\tilde{q}_{\text{n}} \in Q_{\text{near}}} [\mathcal{A}(\tilde{q}_{\text{n}}) + \mathcal{H}(\tilde{q}_{\text{new}}, \tilde{q}_{\text{n}})]$
10 $\quad$ $\mathcal{A}(\tilde{q}_{\text{new}}) \leftarrow \max [\mathcal{T}_{\text{alt}}(\tilde{q}_*, \tilde{q}_{\text{new}}), \mathcal{A}(\tilde{q}_*) + \mathcal{H}(\tilde{q}_{\text{new}}, \tilde{q}_*)]$
11 $\quad$ $\boldsymbol{V} \leftarrow \boldsymbol{V} \cup \{\tilde{q}_{\text{new}}\}; \boldsymbol{E} \leftarrow \boldsymbol{E} \cup \{(\tilde{q}_*, \tilde{q}_{\text{new}})\}$
12 $\quad$ $G \leftarrow$ Rewire(Q_{near}, G)
13 $\quad$ $G \leftarrow$ RemoveUnreachableSamples(G)
14 $Q_{\text{near}} \leftarrow$ Near($\tilde{q}_{\text{act}}, G$)
15 $\tilde{q}_{\text{best}} \leftarrow \arg\min_{\tilde{q}_{\text{n}} \in Q_{\text{near}}} [\mathcal{A}(\tilde{q}_{\text{n}}) + \mathcal{H}(\tilde{q}_{\text{act}}, \tilde{q}_{\text{n}})]$
16 $\Gamma \leftarrow$ RetrieveFinalTrajectory($\tilde{q}_{\text{act}}, \tilde{q}_{\text{best}}, G$)

In the first step of the tree expansion, a random sample is generated in the procedure `InformedSample()` on the basis of the informed strategy adopted from [Gammell et al., 2014]. Samples are generated within an elliptical region to exclude the samples without a chance for improving the solution. Moreover, the process is modified to be able to handle multiple landing sites as follows.

Let $\mathcal{A}(\tilde{q}_{\text{act}})$ be the current minimum safe altitude from the current configuration $\tilde{q}_{\text{act}}$ to the selected best landing site. Random samples are generated for each landing site separately, however, all generated samples have to satisfy the condition

$$\mathcal{A}(\tilde{q}_{\text{act}}) \geq -\tan\theta_{\max}^g \left[\mathcal{E}(\tilde{q}_{\text{act}}, \tilde{q}_{\text{rand}}) + \mathcal{E}(\tilde{q}_{\text{rand}}, \tilde{q}^{\xi_i}) \right] + \mathcal{T}_{\text{alt}}(\xi_i) - \delta_{\mathcal{A}}, \qquad (6.5)$$

where $-\tan\theta_{\max}^g$ is the maximum possible glide ratio, $\mathcal{E}(\cdot, \cdot)$ denotes the Euclidean distance between two configurations, $\mathcal{T}_{\text{alt}}(\xi_i)$ stands for the altitude of the landing site, and $\delta_{\mathcal{A}}$ is a coefficient compensating aircraft movement during the planning process by slightly extending

the ellipse. An example of such ellipses in case of two possible landing sites at the same altitude is depicted in Fig. 6.1. After a new random sample $\tilde{q}_{\text{new}}$ is generated, a nearest possible tree node is determined based on the length of the 2D Dubins maneuver in the `Nearest()` procedure. If the maneuver to the nearest node is longer than the maximum tree growth length Δ_{max}, the maneuver is shortened, and a new sample $\tilde{q}_{\text{new}}$ is generated at its end. This process is done by the `Steer()` procedure. Notice that the maneuver is growth in an opposite direction than aircraft would fly. After that, the best predecessor to the new random sample $\tilde{q}_{\text{new}}$ is found within a set of k_{nn} possible candidates generated by the `Near()` procedure. The predecessor is chosen such that it minimizes the required altitude $\mathcal{A}$ for the new sample $\tilde{q}_{\text{new}}$ which is influenced mainly by the terrain altitude beneath the maneuver, the altitude loss $\mathcal{H}$ to the predecessor sample, and the predecessor minimum safe altitude.

The ability to improve the solution with increasing number of samples in the proposed RRT*-based algorithm is maintained by the `Rewire()` procedure which checks if the newly inserted node $\tilde{q}_{\text{new}}$ can improve the minimum safe altitude $\mathcal{A}$ for any subsequent samples. All the k_{nn} nearest samples from the neighborhood Q_{near} of the inserted sample $\tilde{q}_{\text{new}}$ are tried to be connected to it during the `Rewire()` procedure to minimize their altitude $\mathcal{A}$. Notice that all connections have to be tested for collisions with the terrain and obstacles given by $\mathcal{T}_{\text{alt}}$. Notice that the memory consumption of the proposed algorithm is reduced by pruning the roadmap. All the samples which are not reachable anymore by the aircraft are removed from the roadmap in the `RemoveUnreachableSamples()` procedure. This procedure helps the algorithm to run during the whole flight.
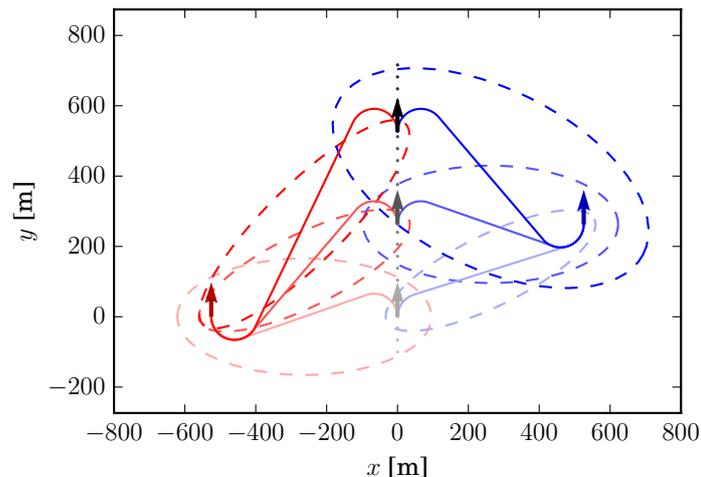

Figure 6.1: An example of the time evolution of the elliptical sampling regions for two landing sites (ξ_1 in red and ξ_2 in blue) for three different positions of the aircraft flying along the black dotted trajectory. No terrain nor obstacles are considered. The minimum safe altitude $\mathcal{A}$ is determined by the shorter Dubins maneuver. Notice that some of the red maneuvers are outside their sampling regions which is caused by $\mathcal{A}$ because the blue maneuver is significantly shorter, and thus the red trajectory cannot be optimal.

6.3   Tree Performance

The performance of the proposed method is strongly influenced by used parameter values. The most influencing parameters are the number of k_{nn} nearest chosen samples and the maximum expansion length Δ_{max}. Two consequences are measured – the number of generated nodes n

and their inequality. Nodes are generated within an informed ellipse. Denote the number of nodes lying closer to the landing site as n_ξ and the number of nodes lying closer to the aircraft as n_a. The tree is growth from the landing site, therefore, all generated nodes are closer to the landing site at the beginning. As the tree grows, nodes are generated even closer to the aircraft. Thus, we denote $\frac{n_\xi - n_a}{a}$ as the nodes inequality. The inequality is 1 at the beginning and then it decreases to 0. Tree performances based on these parameters values are compared in Fig. 6.2 and examples of such trees are depicted in Fig. 6.3.

Based on these measurements, we have decided to use the following values

$$k_{nn} = 70, \qquad \Delta_{max} = 300 \text{ m}. \tag{6.6}$$

Even though it might seems as ineffective values based on Fig. 6.3, the opposite is the truth. These values provide a compromise between the quality of solutions and the roadmap growth speed. Smaller values of k_{nn} causes the roadmap to be too winding and the final trajectory would have to be processed much more. Higher values of this parameter causes the roadmap to grow too slowly. Shorter maximum growth step causes too slow growth of the roadmap, longer maximum steps causes the roadmap to not be smooth enough.


(a) Number of nodes
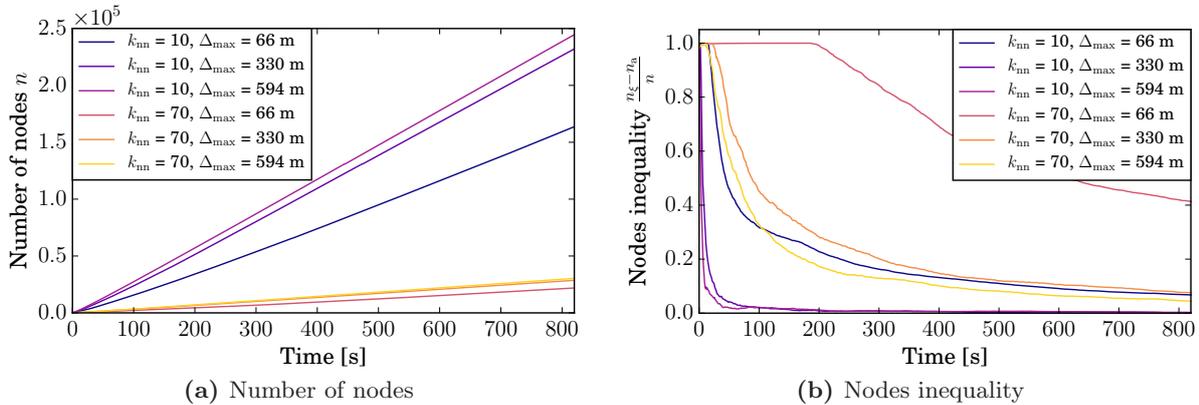
(b) Nodes inequality

Figure 6.2: A comparison of tree performances based on the parameter values. Nodes are generated within an informed ellipse. The time evolution of the number of nodes n is shown in (a) and corresponding nodes inequality is shown in (b), where n_ξ denotes the number of nodes lying closer to the landing site and n_a denotes the number of nodes lying closer to the aircraft.

6.4 Retrieving a Final Trajectory

When the aircraft experiences the loss of thrust, the expansion of the roadmap is terminated, and the final trajectory is retrieved. This process is analogous to the insertion of a new sample into the roadmap, but in this case, the whole trajectory is retrieved. First, the best predecessor sample from the roadmap has to be determined. Hence, k_{nn} best neighbor samples to the actual position of the aircraft are chosen from the graph G into a set Q_{near}. The best predecessor sample is chosen from this set such that it minimizes the required minimum altitude $\mathcal{A}$ for the actual position of the aircraft. Secondly, the trajectory has to be retrieved from the roadmap. This is done by the `RetrieveFinalTrajectory()` procedure which can optionally provide final adjustments to the trajectory as well, e.g., its smoothing.

Because only a limited number of the closest samples from the roadmap is checked, the final trajectory is retrieved almost instantly (approx. in 80 ms) providing the safest emergency landing trajectory whenever it is needed.

(a) $k_{nn} = 10$, $\Delta_{max} = 66$ m, 1789 nodes

(b) $k_{nn} = 10$, $\Delta_{max} = 330$ m, 2014 nodes

(c) $k_{nn} = 70$, $\Delta_{max} = 66$ m, 278 nodes

(d) $k_{nn} = 70$, $\Delta_{max} = 330$ m, 264 nodes
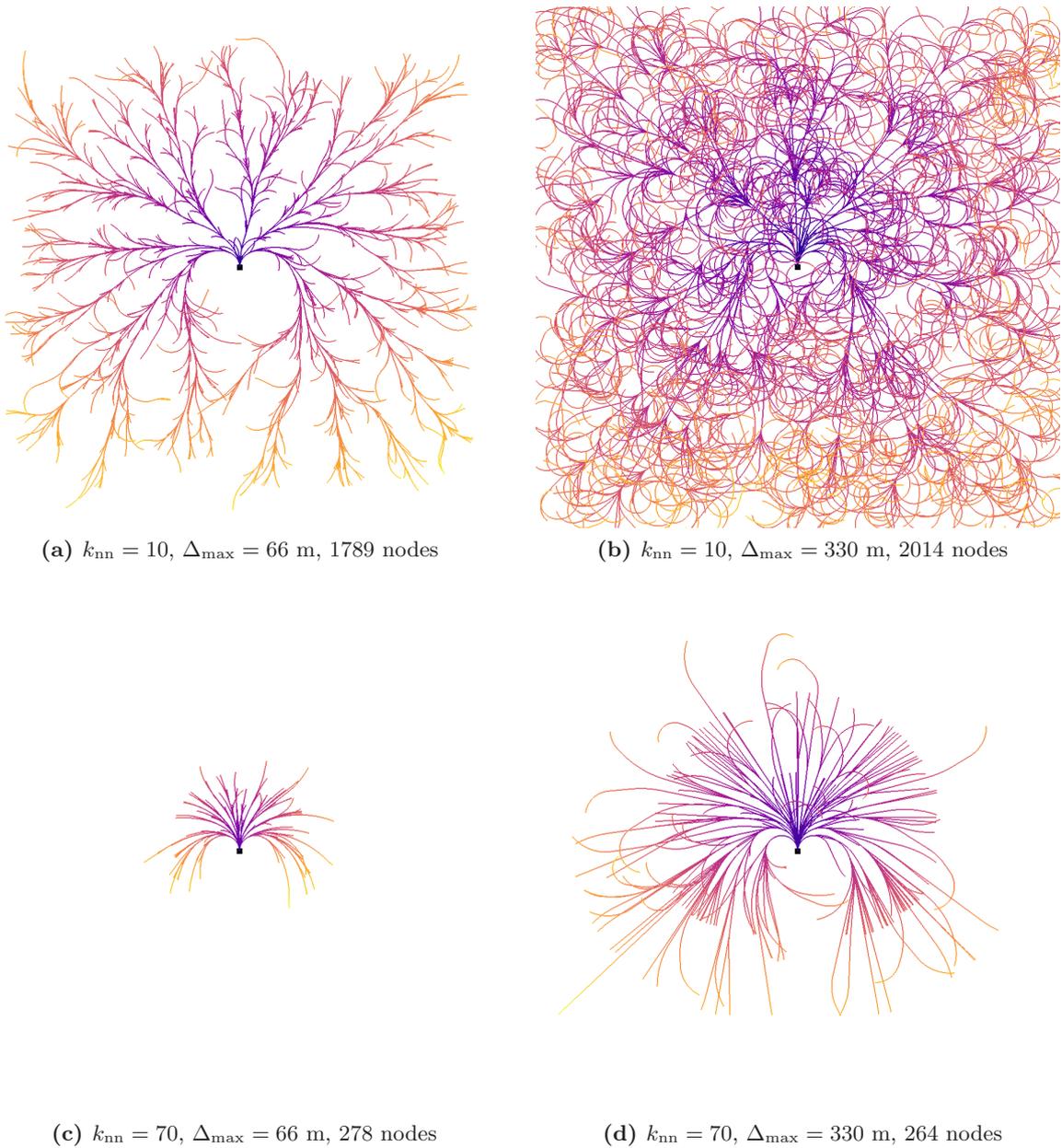
Figure 6.3: Examples of tree grown for 30 s in a rectangle of 1,000 x 1,000 meters with different parameter values. It is clearly visible that the number of the tested nearest neighbors and the maximum allowed tree growth length during the insertion of the new nodes into the roadmap strongly influence its performance in terms of the number of inserted nodes, covered area, and the roadmap branching. These properties have influenced the solution quality as well.

7

Evaluation of the Proposed Method

We have proposed a novel approach to the emergency landing path planning in a case of the engine malfunction. In this chapter, we report on the achieved results and present found solutions to demonstrate the properties of the proposed algorithm.

7.1 Scenarios

We have prepared two scenarios for evaluation of the proposed method. The first one, referred to as *Volcano*, is an artificially made scenario consisting of a conical volcano with the altitude of approx. 1,000 m at the center of the environment. The volcano is surrounded by a relatively flat terrain with a varying altitude between 0 m and 250 m. Moreover, this scenario includes several no-flight zones with heights from 450 to 750 meter and radii in between 100 and 250 meters. These zones are placed within 2.7 km from the volcano center. The scenario features single bi-directional runway with oppositely oriented landing sites ξ_1 and ξ_2 located near the volcano. The aircraft is flying on a circular trajectory around the volcano at the altitude of 800 m. Hence, the aircraft cannot overfly the volcano. The scenario is visualized in Fig. 7.1.

The second scenario is referred to as *Courchevel* and it is a real scenario based on surroundings of Courchevel, France, located in French Alps. The altitude in this scenario varies from 566 through 3,830 meters. There are six airports located in the area; five of them features bi-directional runways and the sixth one, Courchevel Airport, features only a single-directional runway for landing. No arbitrary obstacles nor flight zones have been added into this scenario. The flight path starts at Courchevel Airport and continues through the valley towards mountains. After overflying them, the aircraft turns back and returns to the Courchevel Airport through the other valley. Courchevel is a very popular ski resort, and so we have chosen this path to reflect a possible sightseeing flight. The scenario is visualized in Fig. 7.2.

7.2 Experiments

Thirteen configurations $\{q_0, \ldots, q_{12}\}$ are chosen equidistantly along the aircraft trajectories such that the aircraft visits the configuration q_0 at time 0 s and the configuration q_{12} is at the final point of the trajectory. A possible engine failure in these configurations is considered for
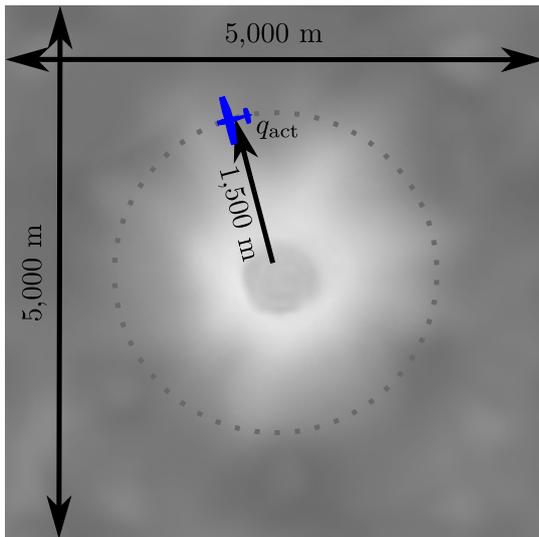
(a) Dimensions in the scenario and the fight path
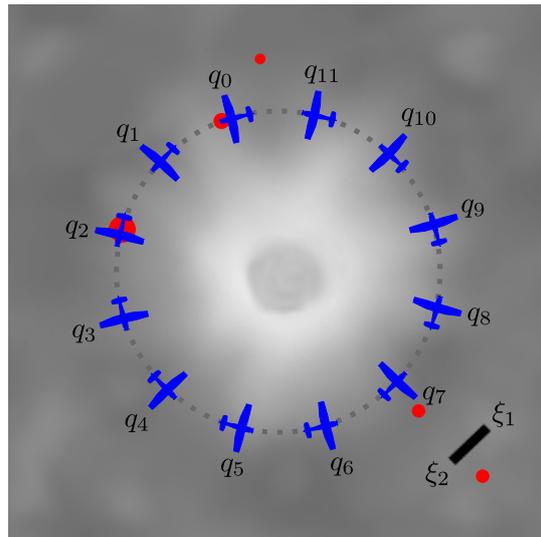
(b) Selected aircraft configurations, no-flight zones and possible landing sites

Figure 7.1: A visualization of the scenario *Volcano*. The flight path is shown by a dotted line, no-flight zones are shown as red obstacles, possible landing sites ξ_1 and ξ_2 are located on the single bi-directional runway depicted by a black rectangle and chosen engine failure positions $q_0, \ldots, q_{11}$ are shown as well. The terrain is represented by a grayscale height map ranging from 0 through 1,000 meters. Note that the aircraft outlines and runway have been enlarged and they are not in scale.
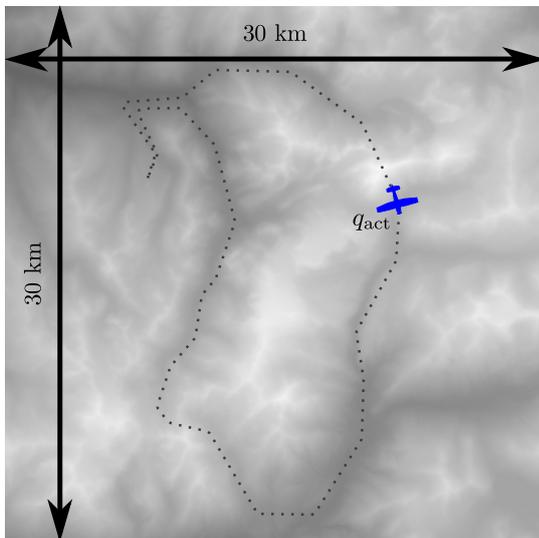

(a) Dimensions in the scenario and the fight path
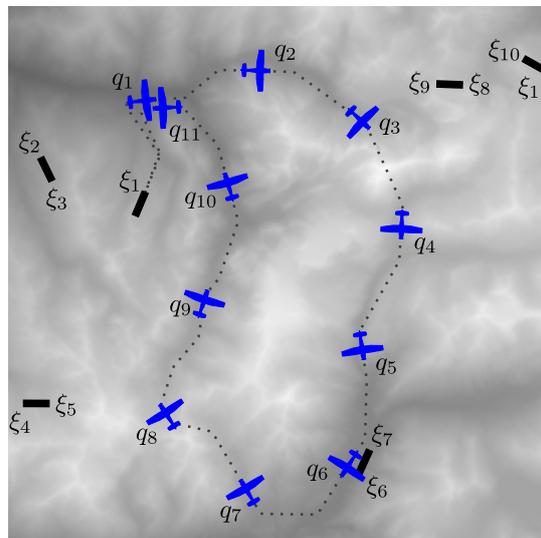
(b) Selected aircraft configurations and possible landing sites

Figure 7.2: A visualization of the scenario *Courchevel*. The scenario is based on a height map of area around Courchevel, France, obtained from [JPL NASA, 2018]. It is shown as a grayscale height map ranging from 566 through 3,830 meters. An aircraft flight path is shown by a dotted line, possible landing sites ξ_i are depicted as the black rectangles and tested engine failure positions $q_1, \ldots, q_{11}$ are shown, too. Note that the aircraft outlines and runways have been enlarged and they are not in scale.

the comparison between the any-time version of the proposed algorithm and its single-query version with different planning times.

In the scenario Volcano, the last configuration q_{12} is omitted as it is identical to the first configuration q_0. The path is flown three times, i.e., the aircraft makes three circles around the volcano to compare the time evolution of the solution of the proposed method. In Courchevel scenario, the first and last configurations q_0 and q_{12} are omitted as they correspond to the Courchevel Airport. The path is flown only once.

The any-time version of the proposed method is compared with its single-query version in which the planning process is started for the fixed time at the time of the engine failure. We use 0.05 s, 0.5 s, 1 s, 2 s, 5 s and 10 s planning times for the single-query version. The roadmap of the planning tree is made of 3D maneuvers based on 2D Dubins maneuvers, as described in Sec. 4.3.1. The described optimization of the turning radii (4.27) to achieve the minimum altitude loss is done as follows. Ten discrete turning radii $R_i \in [R_{min}, 5R_{min}]$ are considered to be used in maneuvers. During the optimization, all possible combinations are examined and the best maneuver from all 100 possibilities is chosen as the optimal one.

Experiments have been performed 40 times on a single core of the AMD Phenom II X6 1090T CPU running at 3.2 GHz. Examples of found solutions are shown in Fig. 7.3 and results are depicted in Fig. 7.4.
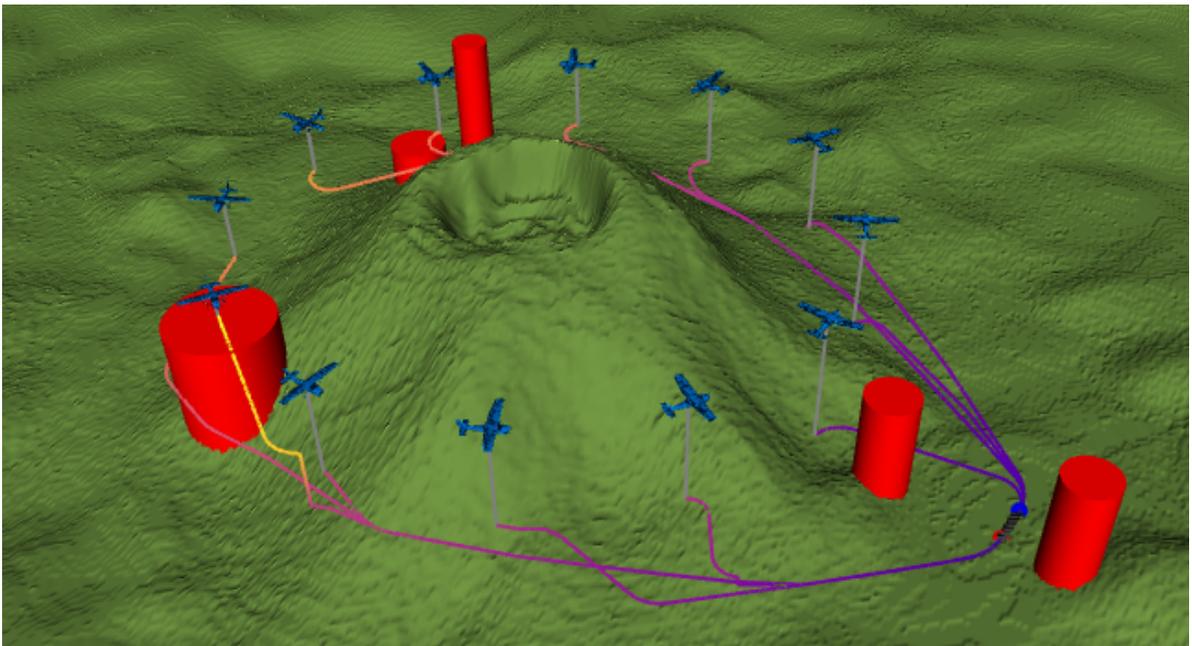

Figure 7.3: An example of the found trajectories for 12 selected configurations $(q_0, \ldots, q_{11})$ for the scenario Volcano. All the trajectories have been retrieved by the proposed any-time algorithm during the third round around the volcano.

7.3 Results

Although the aircraft can land safely from any position along its trajectories, the single-query version of the solver is unable to find a feasible solution if the dedicated time to find a solution is too short. In such cases, the minimum required altitude is higher than the current altitude of the aircraft.

At the beginning, the proposed algorithm provides similar results as the single-query version. The reason is that the roadmap is not pre-computed yet. After a short time, the roadmap is built dense enough and the proposed algorithm provides the best results. As we can see from the results depicted in Fig. 7.4a, they do not improve with time, i.e., the results are still the same regardless the number of rounds around the volcano. Since the time the roadmap is dense enough, the proposed algorithm can provide a high-quality solution almost instantly.

The single-query version can provide results of similar quality. However, if there is not a direct visibility to the landing site, the single-query version has problems with finding a solution of reasonable quality. In some cases, it can return even an unfeasible solution. Moreover, the quality of the solution is dependent on the planning time. In some cases, the shorter the planning time is, the better solution is found. In other cases the behavior is opposite. Therefore, the question is which planning time should we use, nevertheless, we cannot tell it in advance.
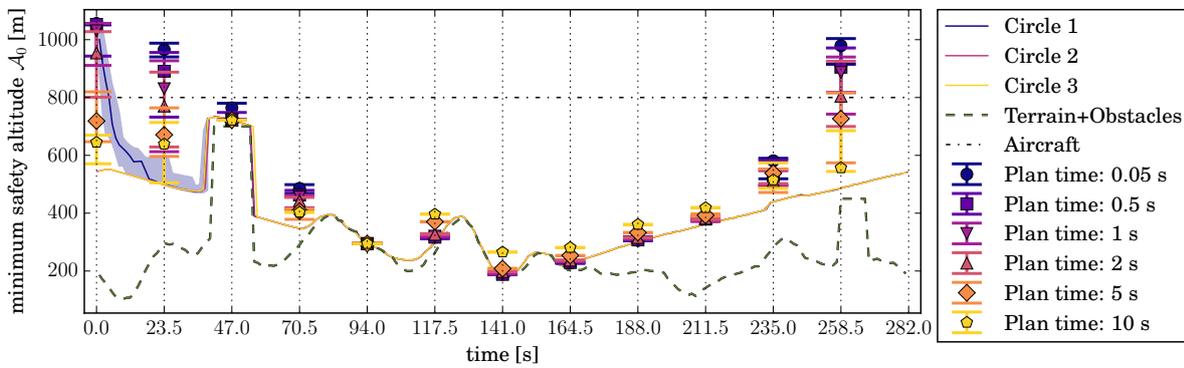
(a) Scenario Volcano
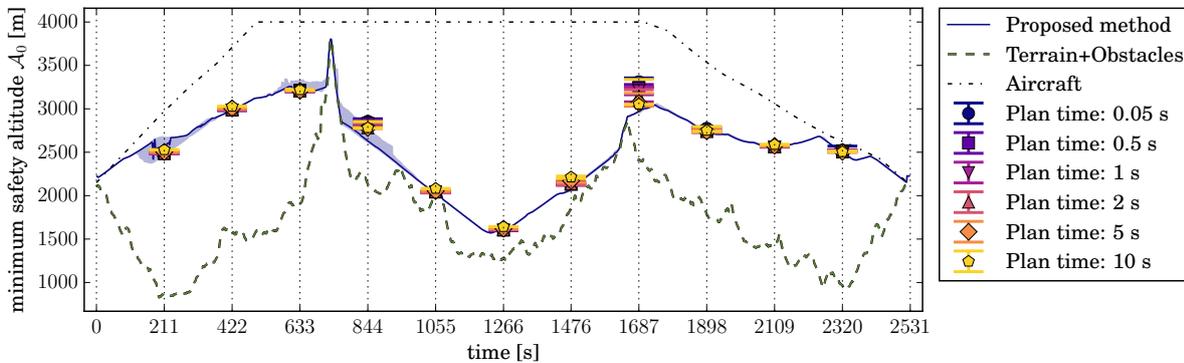
(b) Scenario Courchevel

Figure 7.4: The minimum safe altitude obtained by the proposed any-time algorithm and its single-query version for different planning times. The median and 90% non-parametric confidence interval from 40 trials are shown. The altitude of the terrain/obstacles and the flight level of the aircraft are shown as well. If the minimum safe altitude of the found solution is higher than the actual altitude of the aircraft, no feasible solution was found.

The results confirm the proposed any-time algorithm combines advantages of both the single-query planning to find a high-quality solution but with the faster response than the pure single-query planning. Therefore, there is no need to select the optimal computational time since the roadmap is expanding continuously during the flight.

Conclusion

In this thesis, we study the path planning problem for emergency landing with fixed-wing aircraft experiencing the total loss of thrust. We propose a novel RRT*-based algorithm for planning safe gliding emergency landing trajectories. We consider a model of the gliding aircraft to plan feasible trajectories, and we use Cessna 172 for the numerical evaluation of the model. The proposed solution outperforms its single-query variant because it considers all possible landing sites simultaneously and the motion planning roadmap is continuously updated during the whole flight. If the total loss of thrust occurs, the best landing site and gliding emergency landing trajectory are retrieved almost instantly. Therefore, pilots can start the emergency landing immediately and save the precious altitude. Moreover, the proposed solution gives them a chance to solve other issues, such as bad weather conditions, instead of selecting the best landing site. The proposed algorithm generates a map of the required altitude allowing a safe gliding emergency landing as its byproduct. This map can be used for informing pilots about the number of reachable landing sites if the loss of thrust occurs. Moreover, the map can be used for raising a warning to pilots about entering the area from which they would not be able to land safely if the total loss of thrust occurs, and so they should climb to a safe altitude.

In our future work, we would like to validate the proposed method on a real Cessna 172 or similar type of aircraft. Besides, we aim to utilize the minimum safety altitude map in trajectory planning of complex UAVs missions. For example, imagine a surveillance mission in which the aircraft is requested to patrol over an area or to follow some target. It is a reasonable requirement for the aircraft to be able to safely land at a landing site if it loses the thrust totally in any moment of the mission. The minimum safety altitude map provided by the proposed solution can be used for such a constrained trajectory planning.

Bibliography

[Adler et al., 2012] Adler, A., Bar-Gill, A., and Shimkin, N. (2012). Optimal flight paths for engine-out emergency landing. In *24th Control and Decision Conference*, pages 2908–2915. IEEE.

[Atkins, 2010] Atkins, E. (2010). Emergency landing automation aids: an evaluation inspired by us airways flight 1549. In *AIAA Infotech@ Aerospace*, page 3381.

[Beard and McLain, 2012] Beard, R. W. and McLain, T. W. (2012). *Small unmanned aircraft: Theory and practice.* Princeton university press.

[CASA, 2007] CASA (2007). *Visual Flight Rules Guide.* Canberra: Civil Aviation Safety Authority Australia (CASA).

[Chaudhari et al., 2014] Chaudhari, M., Vachhani, L., and Banerjee, R. (2014). Towards optimal computation of energy optimal trajectory for mobile robots. *IFAC Proceedings Volumes*, 47(1):82–87.

[Choi et al., 2008] Choi, J., Curry, R., and Elkaim, G. (2008). Path planning based on bézier curve for autonomous ground vehicles. In *World Congress on Engineering and Computer Science 2008, Advances in Electrical and Electronics Engineering-IAENG Special Edition of the*, pages 158–166. IEEE.

[Choudhury et al., 2013] Choudhury, S., Scherer, S., and Singh, S. (2013). RRT*-AR: Sampling-based alternate routes planning with applications to autonomous emergency landing of a helicopter. In *IEEE International Conference on Robotics and Automation*, pages 3947–3952.

[Connors and Elkaim, 2007a] Connors, J. and Elkaim, G. (2007a). Analysis of a spline based, obstacle avoiding path planning algorithm. In *Vehicular Technology Conference*, pages 2565–2569. IEEE.

[Connors and Elkaim, 2007b] Connors, J. and Elkaim, G. (2007b). Experimental results for spline based obstacle avoidance of an off-road ground vehicle. In *ION Global Navigation Satellite Systems Conference, ION GNSS*, pages 25–28.

Bibliography

[Desaraju et al., 2015] Desaraju, V. R., Michael, N., Humenberger, M., Brockers, R., Weiss, S., Nash, J., and Matthies, L. (2015). Vision-based landing site evaluation and informed optimal trajectory generation toward autonomous rooftop landing. *Autonomous Robots*, 39(3):445–463.

[Dubins, 1957] Dubins, L. E. (1957). On curves of minimal length with a constraint on average curvature, and with prescribed initial and terminal positions and tangents. *American Journal of mathematics*, 79(3):497–516.

[Durham, 2013] Durham, W. (2013). *Aircraft flight dynamics and control*. John Wiley & Sons.

[Eng, 2011] Eng, P. (2011). *Path planning, guidance and control for a UAV forced landing*. PhD thesis, Queensland University of Technology.

[FAA, 2016] FAA (2016). *Best Glide Speed and Distance*. FAA-850 16_01.

[Gammell et al., 2014] Gammell, J. D., Srinivasa, S. S., and Barfoot, T. D. (2014). Informed RRT*: Optimal sampling-based path planning focused via direct sampling of an admissible ellipsoidal heuristic. In *IEEE/RSJ International Conference on Intelligent Robots and Systems*, pages 2997–3004.

[Hersman et al., 2010] Hersman, D., Hart, C., and Sumwalt, R. (2010). *Loss of Thrust in Both Engines After Encountering a Flock of Birds and Subsequent Ditching on the Hudson River*. Accident Report NTSB/AAR-10/03, National Transportation Safety Board, Washington DC.

[Humbard and Putman, 2007] Humbard, J. J. and Putman, J. (2007). Flight management system and method for providing navigational reference to emergency landing locations. US Patent 7,167,782.

[IATA, 2017a] IATA (2017a). *Fact Sheet – Aviation Benefits Beyond Borders*. International Air Transport Association.

[IATA, 2017b] IATA (2017b). *Fact Sheet – Industry Statistics*. International Air Transport Association.

[JPL NASA, 2018] JPL NASA (2018). Data from advanced spaceborne thermal emision and radiation (aster) mision. `http://terrain.party/api/export?name=courchevel&box=6.941497,45.486540,6.557097,45.217046`. [Online]. Accesed on: 26 April, 2018.

[Karaman and Frazzoli, 2010] Karaman, S. and Frazzoli, E. (2010). Incremental sampling-based algorithms for optimal motion planning. *Robotics Science and Systems VI*, 104:2.

[Karaman and Frazzoli, 2011] Karaman, S. and Frazzoli, E. (2011). Sampling-based algorithms for optimal motion planning. *The International Journal of Robotics Research*, 30(7):846–894.

[Kenny, 2017] Kenny, J. D. (2017). *26th Joseph T. Nall Report*. Richard G. McSpadden, JR.

[Kuffner and LaValle, 2000] Kuffner, J. J. and LaValle, S. M. (2000). Rrt-connect: An efficient approach to single-query path planning. In *IEEE International Conference on Robotics and Automation*, volume 2, pages 995–1001.

[LaValle, 1998] LaValle, S. M. (1998). Rapidly-exploring random trees: A new tool for path planning.

[Lockwood, 1985] Lockwood, G. H. (1985). *Final Report of the Board of Injury: Investigating the Circumstances of an Accident Involving the Air Canada Boeing 767 Aircraft C-GAUN that Effected an Emergency Landing at Gimli, Manitoba on the 23rd Day of July, 1983.* Government of Canada.

[McClamroch, 2011] McClamroch, N. H. (2011). *Steady aircraft flight and performance.* Princeton University Press.

[Mejias and Fitzgerald, 2013] Mejias, L. and Fitzgerald, D. (2013). A multi-layered approach for site detection in uas emergency landing scenarios using geometry-based image segmentation. In *Unmanned Aircraft Systems, International Conference on*, pages 366–372. IEEE.

[Meuleau et al., 2009] Meuleau, N., Plaunt, C., Smith, D., and Smith, T. (2009). Emergency landing planning for damaged aircraft. In *Proceedings of the 21st Innovative Applications of Artificial Intelligence Conference*, pages 3247–3259.

[Meuleau et al., 2011] Meuleau, N. F., Neukom, C., Plaunt, C. J., Smith, D. E., and Smith, T. B. (2011). The emergency landing planner experiment.

[Nuic, 2015] Nuic, A. (2015). User manual for the base of aircraft data (bada) revision 3.13. *Atmosphere*.

[Otte and Frazzoli, 2016] Otte, M. and Frazzoli, E. (2016). Rrtx: Asymptotically optimal single-query sampling-based motion planning with quick replanning. *The International Journal of Robotics Research*, 35(7):797–822.

[Paul et al., 2017] Paul, S., Hole, F., Zytek, A., and Varela, C. A. (2017). Flight Trajectory Planning for Fixed-Wing Aircraft in Loss of Thrust Emergencies. *arXiv preprint arXiv:1711.00716*.

[Penrose, 2003] Penrose, M. (2003). *Random geometric graphs.* Number 5. Oxford university press.

[Roskam, 1985] Roskam, J. (1985). *Airplane design.* DARcorporation.

[Shapira and Ben-Asher, 2005] Shapira, I. and Ben-Asher, J. (2005). Range maximization for emergency landing after engine cutoff. *Journal of aircraft*, 42(5):1296–1306.

[Turnbull, 1999] Turnbull, A. (1999). The typical general aviation aircraft.

[Yang and Sukkarieh, 2008] Yang, K. and Sukkarieh, S. (2008). 3d smooth path planning for a uav in cluttered natural environments. In *IEEE/RSJ International Conference on Intelligent Robots and Systems*, pages 794–800.